



Vansco, M. F., Caravan, R. L., Zuraski, K., Winiberg, F. A. F., Au, K., Trongsirawat, N., Walsh, P. J., Osborn, D. L., Percival, C. J., Khan, M. A. H., Shallcross, D. E., Taatjes, C. A., & Lester, M. I. (2020). Experimental Evidence of Dioxole Unimolecular Decay Pathway for Isoprene-Derived Criegee Intermediates. *The journal of physical chemistry. A*, 2020(124), 3542 - 3554.
<https://doi.org/10.1021/acs.jpca.0c02138>

Peer reviewed version

Link to published version (if available):
[10.1021/acs.jpca.0c02138](https://doi.org/10.1021/acs.jpca.0c02138)

[Link to publication record in Explore Bristol Research](#)
PDF-document

This is the author accepted manuscript (AAM). The final published version (version of record) is available online via American Chemical Society at <https://doi.org/10.1021/acs.jpca.0c02138> . Please refer to any applicable terms of use of the publisher.

University of Bristol - Explore Bristol Research

General rights

This document is made available in accordance with publisher policies. Please cite only the published version using the reference above. Full terms of use are available:
<http://www.bristol.ac.uk/red/research-policy/pure/user-guides/ebr-terms/>

A: Kinetics, Dynamics, Photochemistry, and Excited States

**Experimental Evidence of Dioxole Unimolecular Decay
Pathway for Isoprene-Derived Criegee Intermediates**

Michael F Vansco, Rebecca L Caravan, Kristen L Zuraski, Frank A. F. Winiberg,
Kendrew Au, Nisalak Trongsiwat, Patrick J. Walsh, David L. Osborn, Carl J Percival,
M Anwar H. Khan, Dudley E Shallcross, Craig Allen Taatjes, and Marsha I. Lester

J. Phys. Chem. A, **Just Accepted Manuscript** • DOI: 10.1021/acs.jpca.0c02138 • Publication Date (Web): 07 Apr 2020

Downloaded from pubs.acs.org on April 9, 2020

Just Accepted

"Just Accepted" manuscripts have been peer-reviewed and accepted for publication. They are posted online prior to technical editing, formatting for publication and author proofing. The American Chemical Society provides "Just Accepted" as a service to the research community to expedite the dissemination of scientific material as soon as possible after acceptance. "Just Accepted" manuscripts appear in full in PDF format accompanied by an HTML abstract. "Just Accepted" manuscripts have been fully peer reviewed, but should not be considered the official version of record. They are citable by the Digital Object Identifier (DOI®). "Just Accepted" is an optional service offered to authors. Therefore, the "Just Accepted" Web site may not include all articles that will be published in the journal. After a manuscript is technically edited and formatted, it will be removed from the "Just Accepted" Web site and published as an ASAP article. Note that technical editing may introduce minor changes to the manuscript text and/or graphics which could affect content, and all legal disclaimers and ethical guidelines that apply to the journal pertain. ACS cannot be held responsible for errors or consequences arising from the use of information contained in these "Just Accepted" manuscripts.

Experimental Evidence of Dioxole Unimolecular Decay Pathway for Isoprene-Derived Criegee Intermediates

Michael F. Vansco¹, Rebecca L. Caravan^{2,3,4}, Kristen Zuraski², Frank A. F. Winiberg^{5,6}, Kendrew Au³, Nisalak Trongsiwat¹, Patrick J. Walsh¹, David L. Osborn³, Carl J. Percival⁴, M. Anwar H. Khan⁷, Dudley E. Shallcross⁷, Craig A. Taatjes^{3*}, and Marsha I. Lester^{1**}

¹Department of Chemistry, University of Pennsylvania, Philadelphia, PA 19104-6323, USA.

²NASA Postdoctoral Program Fellow, NASA Jet Propulsion Laboratory, California Institute of Technology, 4800 Oak Grove Drive, Pasadena, CA 91109, USA.

³Combustion Research Facility, Mailstop 9055, Sandia National Laboratories, Livermore, CA 94551, USA.

⁴Chemical Sciences and Engineering Division, Argonne National Laboratory, Lemont, IL 60439, USA.

⁵NASA Jet Propulsion Laboratory, California Institute of Technology, 4800 Oak Grove Drive, Pasadena, CA 91109, USA.

⁶California Institute of Technology, Pasadena, CA 91125, USA.

⁷School of Chemistry, Cantock's Close, University of Bristol, Bristol BS8 1TS, UK.

Abstract

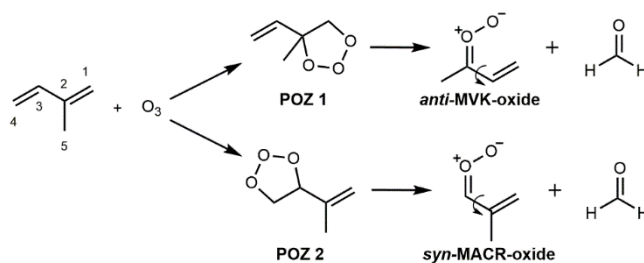
Ozonolysis of isoprene, one of the most abundant volatile organic compounds emitted into the Earth's atmosphere, generates two four-carbon unsaturated Criegee intermediates, methyl vinyl ketone oxide (MVK-oxide) and methacrolein oxide (MACR-oxide). The extended conjugation between the vinyl substituent and carbonyl oxide groups of these Criegee intermediates facilitates rapid electrocyclic ring closures that form 5-membered cyclic peroxides, known as dioxoles. This study reports the first experimental evidence of this novel decay pathway, which is predicted to be the dominant atmospheric sink for specific conformational forms of MVK-oxide (*anti*) and MACR-oxide (*syn*) with the vinyl substituent adjacent to the terminal O atom. The resulting dioxoles are predicted to undergo rapid unimolecular decay to oxygenated hydrocarbon radical products, including acetyl, vinoxy, formyl, and 2-methyl-vinoxy radicals. In the presence of O₂, these radicals rapidly react to form peroxy radicals (ROO), which quickly decay via carbon-centered radical intermediates (QOOH) to stable carbonyl products that are identified in this work. The carbonyl products are detected under thermal conditions (298 K, 10 torr He) using multiplexed photoionization mass spectrometry (MPIMS). The main products (and associated relative abundances) originating from unimolecular decay of *anti*-MVK-oxide and subsequent reaction with O₂ are formaldehyde (88 ± 5%), ketene (9 ± 1%) and glyoxal (3 ± 1%). Those identified from the unimolecular decay of *syn*-MACR-oxide and subsequent reaction of O₂ are acetaldehyde (37 ± 7%), vinyl alcohol (9 ± 1%), methylketene (2 ± 1%), and acrolein (52 ± 5%). In addition to the stable carbonyl products, the secondary peroxy chemistry also generates OH or HO₂ radical co-products.

^{1*} Corresponding author email: cataatj@sandia.gov

^{**} Corresponding author email: milester@sas.upenn.edu

Introduction

Isoprene (2-methyl-1,3-butadiene) is the most abundant volatile organic compound (VOC) emitted into the Earth's atmosphere after methane, with global emissions estimated at ca. 600 Tg year⁻¹.¹ Ozonolysis is an important sink of atmospheric isoprene (ca. 10% globally) that generates reactive carbonyl oxide species called Criegee intermediates.² Unimolecular decay of Criegee intermediates is a significant non-photolytic source of OH radicals, accounting for ca. 1/3 of OH radicals formed in the daytime and essentially all of the OH radicals at night.³⁻⁶ Criegee intermediates have been found to be important tropospheric oxidants themselves, supplementing the oxidation chemistry initiated by OH radicals.⁷ Two four-carbon unsaturated Criegee intermediates, methyl vinyl ketone oxide ((CH₂=CH)(CH₃)COO, MVK-oxide) and methacrolein oxide ((CH₂=C(CH₃))CHOO, MACR-oxide) along with formaldehyde co-product are generated from isoprene ozonolysis via distinct primary ozonide (POZ) intermediates as depicted in Scheme 1. In addition, the simplest Criegee intermediate formaldehyde oxide (CH₂OO) and either methyl vinyl ketone ((CH₂=CH)(CH₃)CO) or methacrolein ((CH₂=C(CH₃))CHOO) are generated from isoprene ozonolysis. The substantial abundance of isoprene in the atmosphere makes understanding the atmospheric fate of MVK-oxide and MACR-oxide of considerable importance. The yields of MVK-oxide and MACR-oxide from isoprene are estimated at 23% and 19%, respectively.²

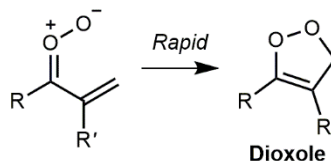


Scheme 1. Formation of MVK-oxide and MACR-oxide Criegee intermediates from isoprene ozonolysis.

The MVK-oxide and MACR-oxide Criegee intermediates are isomers, both having vinyl and methyl substituents, but differing in the position of the methyl groups. Both have extended conjugation involving six π electrons across the vinyl (CH₂=C) and carbonyl oxide (C=O⁺-O⁻) functional groups.⁸⁻⁹ They are

distinctly different than simple saturated carbonyl oxides, such as formaldehyde oxide (CH_2OO) and alkyl-substituted Criegee intermediates, which have four π electron systems ($\text{C}=\text{O}^+ \text{O}^-$).⁸⁻¹⁶ In addition, MVK-oxide and MACR-oxide each have four conformational forms with similar predicted ground state energies (within ca. 3 kcal mol⁻¹). The four conformational forms are separated into two groups based on: (1) the orientation of the terminal oxygen with respect to the vinyl group (*syn* and *anti*), and (2) the orientation of the vinyl group with respect to the $\text{C}=\text{O}$ group (*cis* and *trans*). Under thermal conditions (298 K), the *cis* and *trans* conformations will rapidly interconvert by rotation about the C-C bond (indicated by the curved arrow in Scheme 1).¹⁵⁻¹⁷ The *syn* and *anti* configurations do not interconvert at ambient temperature due to high barriers for rotation about the $\text{C}=\text{O}$ bond and are treated as distinct chemical species with different unimolecular and in some cases bimolecular reaction pathways.^{15, 17-19} The product branching from isoprene ozonolysis has been investigated using master equation modeling,¹⁸⁻²⁰ yielding results that differ depending on the theoretical method used. The most recent calculations give relative abundances for *syn* and *anti* conformers of MVK-oxide and MACR-oxide of ca. 1:1 and 1:4 (298 K, 760 torr), respectively.¹⁸⁻¹⁹

Several unimolecular decay pathways are predicted for MVK-oxide and MACR-oxide, which are highly dependent on their conformational forms.^{15, 17-19, 21} Thus far, only the 1,4 H-atom transfer pathway for *syn*-MVK-oxide to OH products has been experimentally observed.¹⁵ Here, we identify the unimolecular decay pathway predicted for the specific conformations displayed in Scheme 1, in which the terminal oxygen is oriented toward the vinyl group (*anti*-MVK-oxide and *syn*-MACR-oxide).¹⁸⁻¹⁹ For these conformers, the extended conjugation facilitates rapid electrocyclic ring closure that forms a 5-membered cyclic peroxide, known as a dioxole. The ring closure mechanism is illustrated in Scheme 2.



Scheme 2. Electrocyclic ring closure of *anti*-MVK-oxide and *syn*-MACR-oxide to dioxole intermediates.

Here, R and R' indicate the position of the methyl group in MVK-oxide and MACR-oxide, respectively, and in the dioxole product resulting from rapid isomerization. This novel mechanism is predicted to be rapid under thermal conditions for both *anti*-MVK-oxide and *syn*-MACR-oxide. (2140 s^{-1} and 2500 s^{-1} , respectively, 298 K, 760 torr).^{15, 17} These thermal decay rates are representative of a Boltzmann distribution of *cis* and *trans* conformers due to their rapid interconversion.¹⁵⁻¹⁷

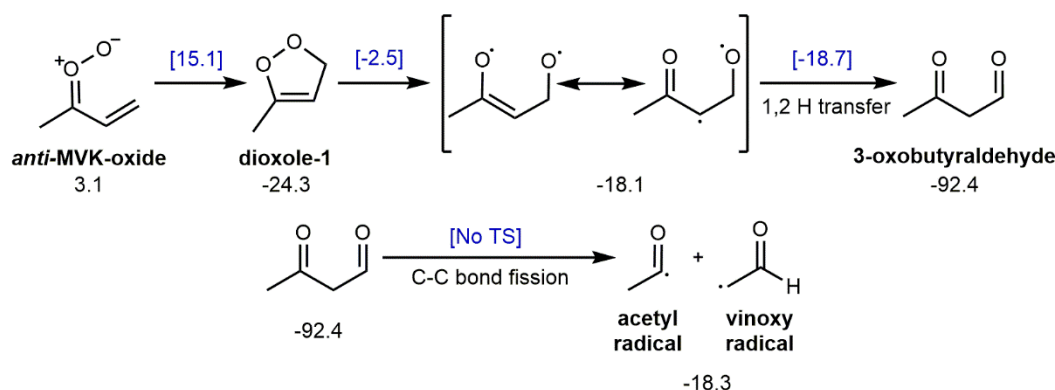
Rapid unimolecular decay via the dioxole pathway is expected to dominate the atmospheric loss of the *anti*-MVK-oxide and *syn*-MACR-oxide Criegee intermediates. The bimolecular chemistry of *anti*-MVK-oxide and *syn*-MACR-oxide is predicted to be similar to that of *syn*-MVK-oxide, which has been recently investigated through direct measurements and theory with H₂O, formic acid, and SO₂ co-reactants.¹⁶ *Syn*-MVK-oxide was found to react slowly with water monomer and dimer (with upper limits of $4.0 \times 10^{-17}\text{ cm}^3\text{ s}^{-1}$ and $3.0 \times 10^{-14}\text{ cm}^3\text{ s}^{-1}$ determined, respectively),¹⁶ in agreement with theoretical predictions.^{16-17, 22} In contrast, *syn*-MVK-oxide reacts rapidly with formic acid ($3.0 \times 10^{-10}\text{ cm}^3\text{ s}^{-1}$) and SO₂ ($4.2 \times 10^{-11}\text{ cm}^3\text{ s}^{-1}$), similar to simple Criegee intermediates.²³⁻²⁶ Typical atmospheric concentrations of H₂O, formic acid, and SO₂ are not large enough for bimolecular reactions to compete with rapid unimolecular decay via the dioxole pathway. Moreover, master equation modeling indicates that isomerization to dioxole under atmospheric conditions (298 K, 760 torr) will account for 42% and 25% of MVK-oxide and MACR-oxide loss, respectively, making the dioxole pathway a significant sink for the four-carbon unsaturated Criegee intermediates formed from isoprene ozonolysis.¹⁸⁻¹⁹ Thus, when evaluating the impact of MVK-oxide and MACR-oxide Criegee intermediates on the atmosphere it is important to characterize the dioxole pathway experimentally, including the final product formed.

This study reports the first experimental evidence of products formed from the unimolecular decay of *anti*-MVK-oxide and *syn*-MACR-oxide Criegee intermediates via the dioxole pathway. Dioxole is predicted to undergo rapid unimolecular decay to radical products (Section II).¹⁵ Under thermal conditions (298 K), and in the presence of excess O₂, these radical products will rapidly add O₂ to form peroxy radicals (ROO) that subsequently undergo unimolecular decay to stable products along with the

formation of an OH or HO₂ radical co-product.²⁷⁻³⁰ The stable products are identified using multiplexed photoionization mass spectrometry (MPIMS) (Section IV). The origin of the identified products is further interrogated via experiments using formic acid as a Criegee intermediate scavenger. The potential atmospheric impact of the dioxole pathway (Section V) is discussed in light of the present experimental findings.

Background

Theoretical studies indicate that electrocyclic ring closure to dioxole is the dominant sink for *anti*-MVK-oxide and *syn*-MACR-oxide Criegee intermediates.¹⁸⁻¹⁹ The full multistep reaction is shown in Scheme 3 for *anti*-MVK-oxide. In Scheme 3, the energies (kcal mol⁻¹) are given relative to *syn-trans*-MVK-oxide (CCSD(T)-F12/CBS-F12(TZ-F12,QZ-F12)//B2PLYP-D3/cc-pVTZ) as reported by Barber *et al.*¹⁵

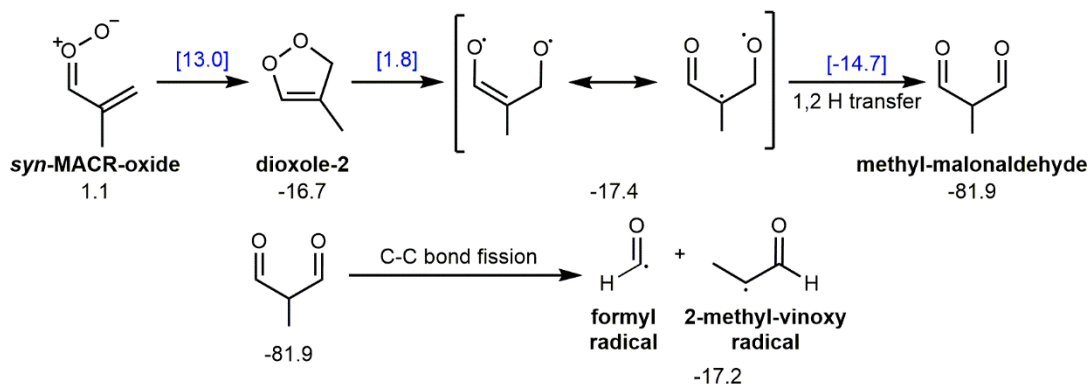


Scheme 3. Unimolecular decay of *anti*-MVK-oxide via electrocyclic ring closure to dioxole-1 and subsequent decay to vinoxy and acetyl radicals. Energies are reported in kcal mol⁻¹ by Barber *et al.*¹⁵

Electrocyclic ring closure forms a 5-membered cyclic peroxide, 3-methyl-4H-1,2-dioxole (dioxole-1). This step is predicted to have a low transition state (TS) barrier (12.0 kcal mol⁻¹) and a fast thermal decay rate (2140 s⁻¹, 298 K, 760 torr).¹⁵ Dioxole-1 is generated with sufficient internal excitation to undergo further rapid unimolecular processes via submerged barriers. Homolytic cleavage of the O-O bond of dioxole-1 forms a diradical, which can rearrange to a closed shell β-dicarbonyl (3-oxobutylaldehyde)

through a highly exothermic ($-74.3 \text{ kcal mol}^{-1}$) intramolecular 1,2 H-atom transfer. This is followed by barrierless C-C bond fission to acetyl radical and vinoxy radical products.¹⁵

An analogous isomerization pathway to dioxole is predicted for *syn*-MACR-oxide, which generates 4-methyl-3H-1,2-dioxole (dioxole-2) as shown in Scheme 4.¹⁹ In Scheme 4, energies (kcal mol^{-1}) are reported by Kuwata *et al.*¹⁹ relative to the lowest energy *anti-trans*-MACR-oxide conformer (CBS-QB3//B3LYP/6-311G(d,p)).



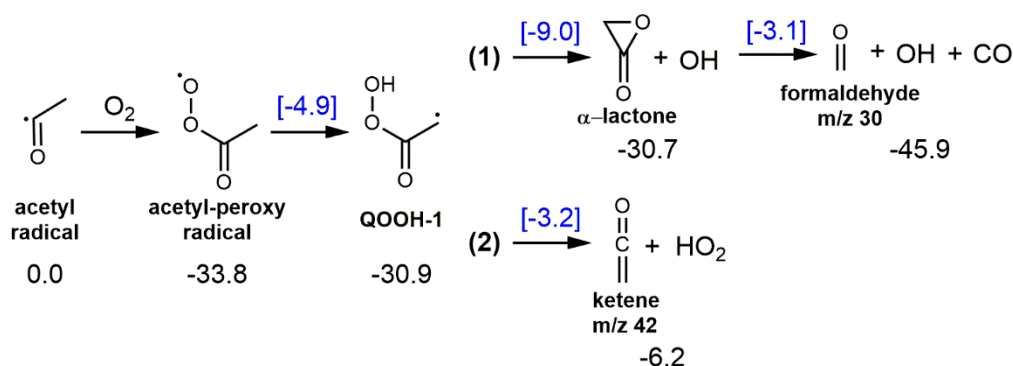
Scheme 4. Unimolecular decay of *syn*-MACR-oxide via electrocyclic ring closure to dioxole-2 and subsequent decay to formyl and 2-methyl-vinoxy radicals. Energies are reported in kcal mol^{-1} by Kuwata *et al.*¹⁹

Electrocyclic ring closure for *syn*-MACR-oxide is also predicted to have a low TS barrier ($11.9 \text{ kcal mol}^{-1}$) and rapid thermal decay rate (2500 s^{-1} , 298 K, 760 torr).¹⁷ Dioxole-2 is expected to undergo similar ring opening and intramolecular isomerization processes that form methylmalonaldehyde in an exothermic reaction (ca. $-65.2 \text{ kcal mol}^{-1}$). In the case of dioxole-2, C-C bond fission results in the formation of formyl radical and 2-methyl-vinoxy radical products. C-C bond fission was not investigated previously.¹⁹ Additional calculations (see SI Sec. S1) demonstrate that sufficient energy is available for dissociation to radical products in an analogous mechanism as that predicted for *anti*-MVK-oxide.

In this study, MVK-oxide and MACR-oxide are generated under thermal conditions (298 K, 10 torr) in the presence of excess O_2 . Under these experimental conditions, the radical products formed through unimolecular decay of MVK-oxide and MACR-oxide via the dioxole channel will rapidly react with O_2 to form ROO.^{28, 31-33} ROO intermediates are predicted to decay rapidly to closed-shell species along with an

OH or HO₂ radical co-product via a hydroperoxyalkyl radical (QOOH) intermediate.²⁸⁻³⁰ Rapid unimolecular decay of ROO is facilitated by internal excitation of the radical products formed in the dioxole pathway, along with exothermic O₂ addition and submerged subsequent barriers that lead to stable products.

Ab initio theoretical studies have examined the radical + O₂ reaction pathways.²⁷⁻³⁰ The mechanisms for product formation from the acetyl radical + O₂ and vinoxy radical + O₂ reaction are shown in Scheme 5 and 6, respectively. For the acetyl radical, O₂ addition generates the acetyl-peroxy radical in an exothermic reaction (-33.8 kcal mol⁻¹).

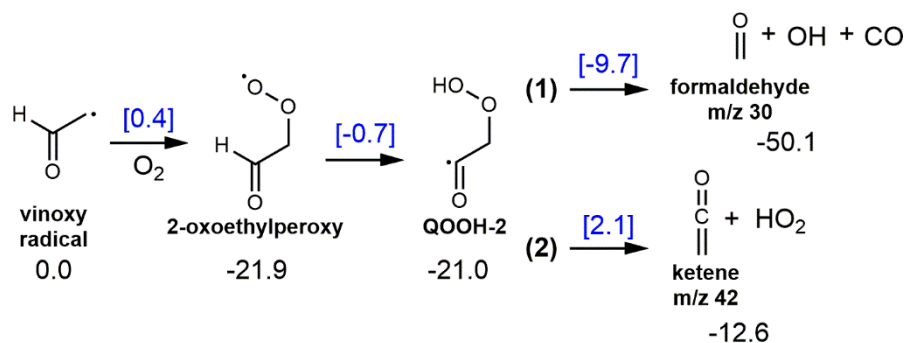


Scheme 5. Reaction of acetyl radical with O₂ and subsequent decay to formaldehyde + OH + CO or ketene + HO₂ products via the QOOH-1 intermediate. Energies are reported by Carr *et al.*, supplemented by the present work, in kcal mol⁻¹.²⁸

The exothermicity of the acetyl radical + O₂ reaction facilitates a 1,4 H-atom transfer from the methyl group to the terminal oxygen atom and results in the formation of QOOH-1. The most energetically favorable decay pathway for QOOH-1 is via a submerged TS barrier (21.9 kcal mol⁻¹) to the cyclic intermediate, α-lactone, and OH co-product. Master equation modeling indicates significant fragmentation of α-lactone to formaldehyde + CO products under low pressure conditions.²⁸ Although the asymptotic energy for the formaldehyde + OH + CO product channel (Scheme 5) was not reported by Carr *et al.*,²⁸ additional calculations (see SI Sec. S1) demonstrate that this is the thermodynamically favored channel. OH yields measured experimentally and predicted using master equation modelling reported in a number of publications together with the low yield of α-lactone directly detected by Chen

and Lee support the dominance of unimolecular decomposition channel over α -lactone stabilization.³⁴⁻⁴³ Ketene + HO₂ products are also energetically accessible, but are expected to be minor due to a higher barrier (27.7 kcal mol⁻¹) to formation. Furthermore, the OH-yield is demonstrated to approach unity at low-pressures (<10 Torr).^{28, 35-37, 39-40} Thus, formaldehyde (along with OH and CO) is expected to be the primary product channel under low pressure conditions.²⁸

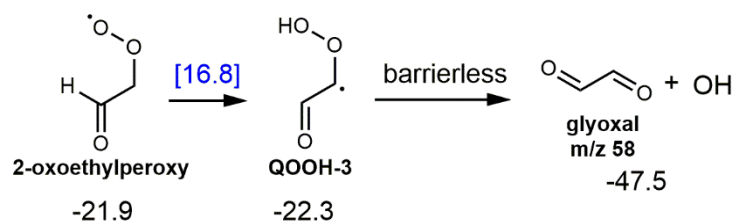
The unpaired electron of vinoxy radicals in the ground state is primarily localized on the carbon,^{29-30, 44-46} which facilitates rapid reaction with O₂ to form ROO.⁴⁷⁻⁴⁸ The vinoxy radical + O₂ reaction generates the 2-oxoethylperoxy radical as shown in Scheme 6. A recent high-level theoretical study of the vinoxy + O₂ reaction predicts formaldehyde + OH + CO to be the dominant product channel, noting other pathways may be minor.²⁹ The proposed mechanism is shown in Scheme 6 and proceeds by O₂ addition to the vinoxy radical via a low barrier (0.4 kcal mol⁻¹) to form the 2-oxoethylperoxy radical in an exothermic reaction (-21.9 kcal mol⁻¹).



Scheme 6. Reaction of vinoxy radical with O₂ and subsequent decay to formaldehyde + OH + CO or ketene + HO₂ via the QOOH-2 intermediate. Energies (kcal mol⁻¹) are reported by Weidman *et al.*²⁹ (CCSD(T)/CBS).

The 2-oxoethylperoxy radical is formed with sufficient energy (21.9 kcal mol⁻¹) to isomerize via a H-atom transfer from the neighboring aldehyde and yield QOOH-2, which can promptly decay via a submerged barrier (11.3 kcal mol⁻¹) to formaldehyde + CO + OH. QOOH-2 can also decay via a higher lying TS barrier (23.1 kcal mol⁻¹) to form ketene + HO₂, which is predicted to be a minor product channel. Alternatively, 2-oxoethylperoxy radical can undergo a 1,3 H-atom transfer via a large barrier (38.7 kcal

mol⁻¹) to form QOOH-3, which will promptly decompose to glyoxal + OH (Scheme 7). Glyoxal formation is unlikely given the large TS barrier to formation of QOOH-3.

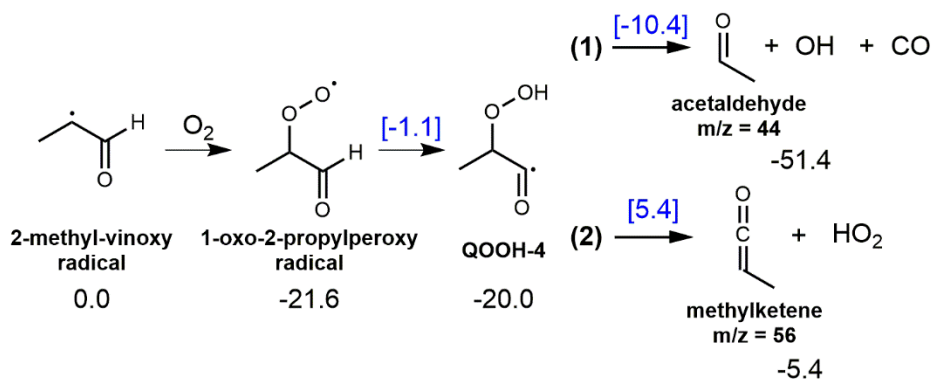


Scheme 7. Alternative decay pathway for 2-oxoethylperoxy radical (formed from vinoxy radical + O₂) to glyoxal + OH via the QOOH-3 intermediate. Energies (kcal mol⁻¹) are reported by Weidman *et al.*²⁹ (CCSD(T)/CBS).

Fewer experimental studies have been conducted to investigate the products from the vinoxy radical + O₂ reaction compared with the corresponding acetyl reaction. Zhu *et al.*⁴⁹ reported that glyoxal may be a reaction product, however the disappearance rate of the vinoxy radical did not match the appearance rate of glyoxal, suggesting that is produced from the decomposition of the 2-oxoethylperoxy radical. Their preliminary results also suggested formaldehyde + CO + OH is a primary product channel.

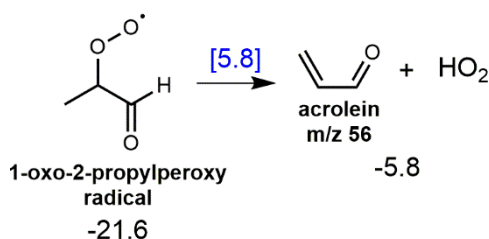
Unimolecular decay of *syn*-MACR-oxide via the dioxole pathway results in formation of formyl radical and 2-methyl-vinoxy radical (Scheme 4), which are both predicted to undergo barrierless addition of O₂ to form the formyl-peroxy radical and 1-oxo-2-propylperoxy radical, respectively. Formyl-peroxy radical is known to undergo prompt decomposition to CO + HO₂,^{27, 50} whereas the products from the 1-oxo-2-propylperoxy radical are less well known.

A recent high-level theoretical study has predicted the products from the 2-methyl-vinoxy + O₂ reaction (Scheme 8 and 9).³⁰ The calculations indicate that 1-oxo-2-propylperoxy will undergo a 1,4 H-atom transfer from the neighboring aldehyde via a submerged barrier (20.5 kcal mol⁻¹) to form QOOH-4 (Scheme 8).



Scheme 8. Reaction of 2-methyl-vinoy radical with O_2 and subsequent decay to acetaldehyde + OH + CO, or methylketene + HO_2 via the QOOH-4 intermediate. Energies (kcal mol⁻¹) are reported by Davis *et al.*³⁰ (CCSD(T)/CBS).

QOOH-4 is anticipated to decompose primarily to acetaldehyde + OH + CO via a submerged barrier (9.6 kcal mol⁻¹). Methylketene + HO_2 products are expected to be a minor channel due to a larger TS barrier to products (25.4 kcal mol⁻¹). Alternatively, 1-oxo-2-propylperoxy radical can undergo direct unimolecular decay to acrolein + HO_2 via a barrier of 27.4 kcal mol⁻¹ (Scheme 9).



Scheme 9. Direct unimolecular decay of 1-oxo-2-propylperoxy radical (formed from 2-methyl-vinoy radical + O_2) to acrolein + HO_2 . Energies (kcal mol⁻¹) are reported by Davis *et al.*³⁰ (CCSD(T)/CBS).

Methods

Experiments are performed using the Sandia Multiplexed Photoionization Mass Spectrometer (MPIMS) apparatus interfaced with the tunable-VUV radiation of the Chemical Dynamics Beamline (9.0.2) of the Advanced Light Source (Lawrence Berkeley National Laboratory).⁵¹⁻⁵² MVK-oxide and MACR-oxide Criegee intermediates are generated in separate experiments from the (Z/E)-1,3-diiodobut-

2-ene or 1,3-diiodo-2-methylprop-1-ene precursor, respectively, as described by Barber *et al.*¹⁵ and Vansco *et al.*⁹.

The relevant precursor is entrained in a He flow using a pressure- and temperature-controlled glass bubbler (298 K, 100 torr). The precursor ($\sim 2\text{--}3 \times 10^{13} \text{ cm}^{-3}$), O₂, ($\sim 6.4 \times 10^{16} \text{ cm}^{-3}$), deuterated formic acid and bath gas (He) are delivered to a halocarbon wax-coated quartz reactor tube maintained at 298 K and 10 torr. Calibrated mass flow controllers are used to obtain specific mixing ratios of reactants. The gaseous mixture is photolyzed along the length of the quartz reactor tube with the 248 nm output of a KrF excimer laser (248 nm, 4 Hz). The laser energy is attenuated (to 100 mJ/pulse at laser output, ~ 20 mJ/pulse through the reactor) using fine meshes in order to reduce the Criegee intermediate concentration (max. $\sim 1 \times 10^{12} \text{ cm}^{-3}$) so that side removal processes are minimized and the unimolecular reactions of the Criegee intermediates can be examined. The total gas flow rate through the reactor is sufficient such that the gas-mixture is entirely replenished between laser pulses. Pulsed UV-photolysis of the precursors generates a resonance-stabilized monoiodoalkenyl radical that subsequently reacts with O₂ to produce the Criegee intermediates.^{9, 15} The gas mixture is continuously sampled through an orifice on the side of the reactor tube and the resultant molecular beam is intercepted orthogonally with the tunable VUV radiation. The ions generated by VUV-ionization are pulse-extracted, accelerated orthogonally, and detected via time-of-flight mass spectrometry. Products resulting from MVK-oxide and MACR-oxide unimolecular decay and subsequent reaction with O₂ are investigated through experiments at a fixed ionization energy of 10.5 eV and photoionization efficiency (PIE) scans (9.0–11 eV). High-resolution mass spectrometry is utilized to identify stable products. For scavenger experiments, sufficient formic acid is added to the reactor tube such that bimolecular reaction with *anti*-MVK-oxide would compete with its unimolecular decay and prevent unimolecular decay products from being formed. Pseudo-first-order conditions were maintained throughout: [O₂] \gg [(Z/E)-1,3-diiodobut-2-ene] and [deuterated formic acid] \gg [MVK-oxide].

Results

A. MVK-oxide

Specific conformers of MVK-oxide (*anti*) and MACR-oxide (*syn*) are predicted to rapidly decay via the dioxole pathway and generate radical products that include acetyl and vinoxy (MVK-oxide, Scheme 3), and formyl and 2-methyl-vinoxy radicals (MACR-oxide, Scheme 4). These radicals react rapidly with O₂ to form ROO (rate constants ca. 10⁻¹³-10⁻¹² cm³ s⁻¹, 298 K).^{28, 31-33} Typical concentrations of O₂ used in the experiment (ca. 6.4 × 10¹⁶ molecules cm⁻³) facilitate rapid ROO formation (ca. μs) compared to the experimental time resolution.⁵¹ The resultant internally excited ROO are expected to undergo rapid unimolecular decay to closed-shell products along with transient OH or HO₂ radical co-products.^{27-30, 33} Stable products anticipated from MVK-oxide decay via the dioxole pathway (and subsequent reaction with O₂) include formaldehyde, ketene, glyoxal, and α-lactone (Section II, Schemes 5-7). Those expected from MACR-oxide decay via the dioxole pathway (and subsequent reaction with O₂) include acetaldehyde, methylketene, and acrolein (Section II, Schemes 8 and 9). The stable products are identified using MPIMS via a combination of high-resolution time-of-flight mass spectrometry, temporal profiles, and spectroscopically via photoionization efficiency (PIE) curves. Addition of a second O₂, following RO₂ isomerization to QOOH, is not anticipated to be substantial under our experimental conditions. Thus, we do not consider subsequent autoxidation products from any of the RO₂ discussed herein.

After photolytic generation of MVK-oxide, formaldehyde (m/z 30), ketene (m/z 42), and glyoxal (m/z 58) are identified as stable products in the MPIMS experiments. The temporal profile associated with m/z 30 (integrated over 8.4-11.0 eV) shows a fast rise followed by a constant photoionization signal consistent with the rapid formation of a stable product (Figure 1, top panel).

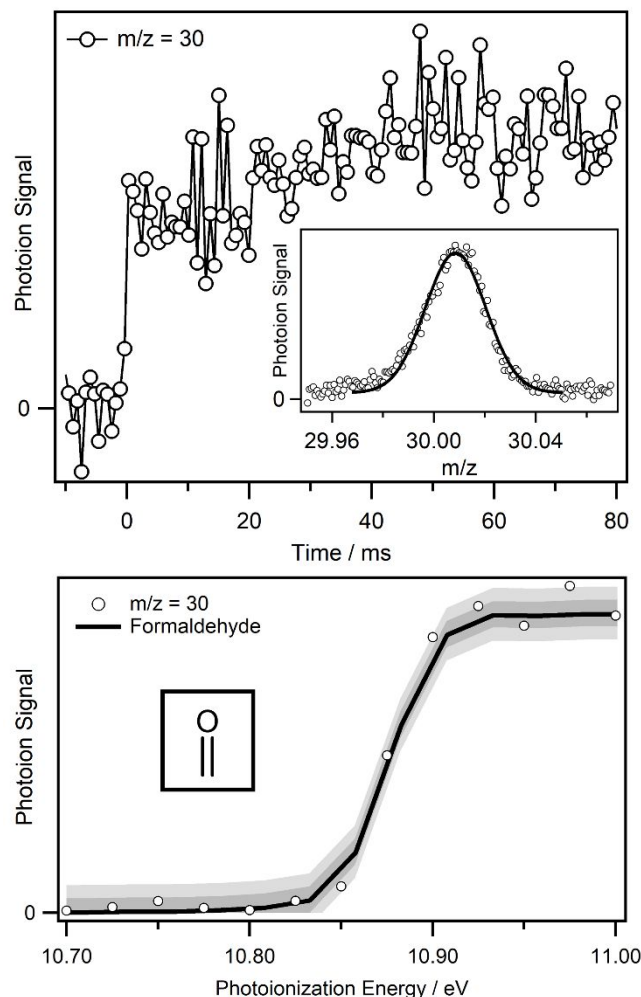


Figure 1. (Top) Temporal profile of m/z 30 mass channel integrated over the 8.0-11.0 eV photoionization energy range. (Inset) High resolution mass spectrum of the m/z 30 signal integrated over the full kinetic time window (0-80 ms) and photoionization energies (8.0-11.0 eV). (Bottom) PIE curve of m/z 30 (open circles) integrated over the full kinetic time window (0-80 ms) compared with the absolute photoionization spectrum of formaldehyde (black line).⁵³ The black lines shows the result of a least squares fit of the absolute photoionization spectrum of formaldehyde to the experimental m/z 30 data. The darker and lighter grey shaded regions represents 1σ and 2σ uncertainty in the fit, respectively.

A Gaussian fit to m/z 30 of the mass spectrum (Figure 1, top panel *inset*) yields an exact mass of 30.011 ± 0.003 amu, consistent with the mass of formaldehyde (30.011 amu). The PIE curve of m/z 30 (open circles) integrated over the full kinetic time window (0-80 ms) is shown in the bottom panel of Figure 1. The appearance energy (10.88 eV)⁵⁴ and shape of the m/z 30 photoionization spectrum matches the absolute photoionization spectrum of formaldehyde (black line),⁵³ confirming its formation in the

experiment. The experimental data are fit to the absolute photoionization spectrum of formaldehyde (black line) via a least squares method. The uncertainty in the fit ($\pm \sigma$, $\pm 2\sigma$) is represented by shaded regions.

Ketene (m/z 42) is expected to be a minor product in the proposed mechanism. The temporal profile and high resolution mass spectrum of the m/z 42 mass channel (8.4-11.0 eV) is shown in Figure 2.

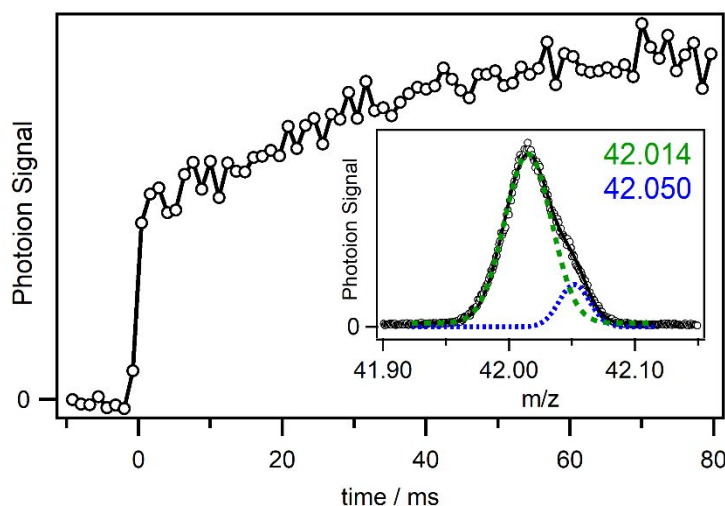


Figure 2. (Inset) High resolution mass spectrum integrated over the full kinetic time window (0-80 ms) and photoionization energies (8.0-11.0 eV) showing a partially resolved feature at m/z 42. The corresponding temporal profile (10.5 eV) shows rapid formation of a stable product following photolytic generation of MVK-oxide.

The temporal profile shows rapid formation of a stable species upon photolysis. The width and asymmetry of the m/z 42 feature in the mass spectrum is indicative of multiple ionized species with the same nominal mass but different numbers of C and O atoms that results in partially resolved peaks. A sum of two Gaussian functions is used to fit the feature (black line) to extract the exact mass of each component. The fit yields an exact mass of 42.014 ± 0.004 amu (green line) and 42.050 ± 0.003 amu (blue line) consistent with the mass of ketene (42.011 amu) and C_3H_6 (42.047 amu), respectively. PIE curves associated with the two different mass regions are shown in Figure 3 (41.95-42.00 and 42.04-42.08 amu) to differentiate between the two species contributing to the m/z 42 photoionization signal.

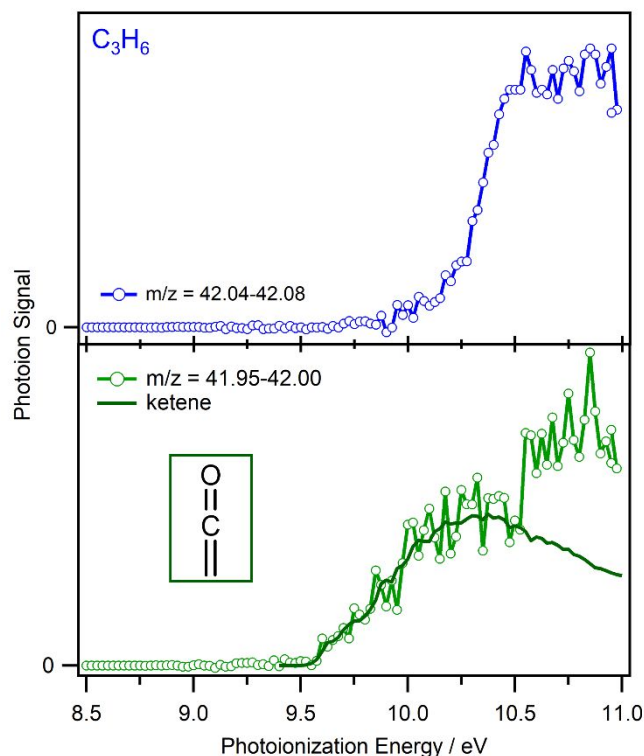


Figure 3. (Top) PIE curve associated with the 42.04-42.08 mass window (blue open circles). All traces are generated by integrating over the full kinetic time window (0-80 ms). (Lower panel) The PIE curve of the 41.95-42.00 mass window (green open circles) is consistent with the known PI spectrum of ketene is shown for comparison (dark green line).⁵⁵ Interference from an unidentified daughter ion is observed at higher photoionization energy (ca. 10.5 eV).

The resultant PIE curves are distinctly different. The appearance energy and shape of the PIE curve associated with the lower mass region (bottom panel, green open circles, ca. 9.6 eV) matches the absolute photoionization spectrum of ketene (dark green line) below 10.5 eV.⁵⁵⁻⁵⁶ At higher photoionization energy (≥ 10.5 eV) the PIE curve changes due to photoionization of an interfering species. Integration of the higher mass region (42.04-42.08, top panel) results in a PIE curve that matches the interfering signal observed in the top panel. The mass of the interfering species (42.049 ± 0.003) is consistent with the chemical makeup of C_3H_6 (42.047) and is attributed to dissociative ionization of a larger species.

Glyoxal and α -lactone (m/z 58) products are predicted for the vinoxy radical + O_2 and acetyl radical + O_2 reactions, respectively. Glyoxal formation is unlikely given a high barrier to formation (38.7 kcal mol⁻¹), while significant fragmentation of α -lactone to formaldehyde + CO is expected due to the

exothermicity of the proposed mechanism. Nevertheless, a weak signal matching the exact mass of glyoxal and α -lactone (58.005) is observed. The temporal profile, high-resolution mass spectrum, and PIE curve of m/z 58 is shown in Figure 4.

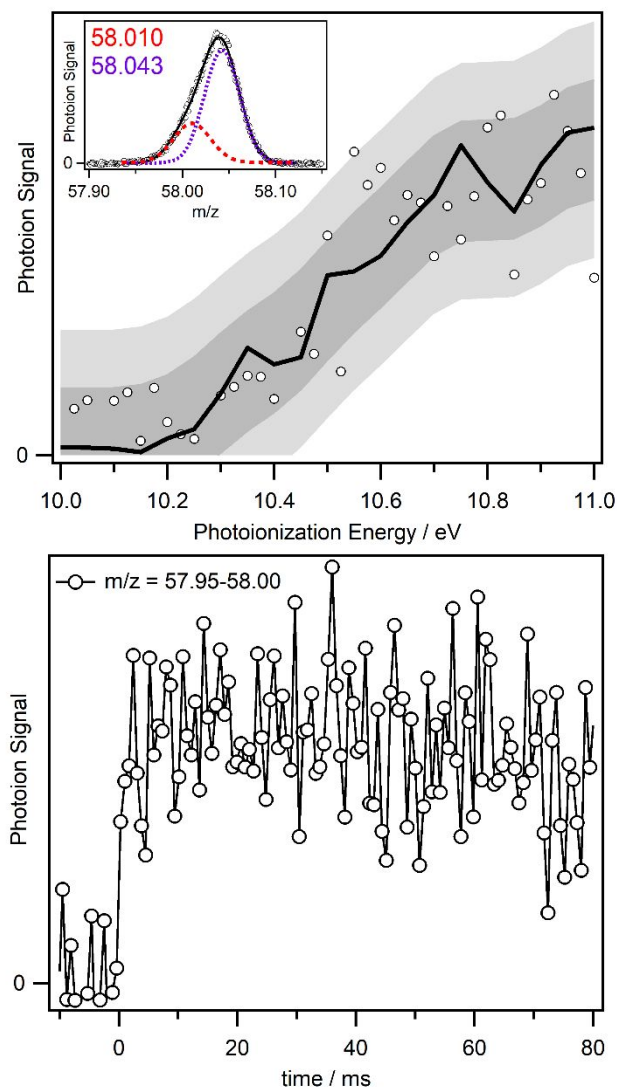


Figure 4. (Top, inset) High-resolution mass spectrum of the m/z 58 signal integrated over the full kinetic time window (0-80 ms) and photoionization energies (8.0-11.0 eV). (Top) Photoionization efficiency curve of m/z 58 (open circles) integrated over 57.95-58.00 amu and the full kinetic time window (0-80 ms) compared with the known photoionization spectrum of glyoxal (black line). (Bottom) Temporal profile of the m/z 57.95-58.00 mass region integrated over the 8.0-11.0 eV photoionization energy range.

The width and asymmetry of the m/z 58 feature in the mass spectrum is indicative of multiple species with the same nominal mass but different numbers of C and O atoms contributing to the photoionization signal. A sum of two Gaussian functions is used to fit the feature (black line) and extract the exact mass

of each component. The fit yields a peak position of 58.010 ± 0.005 amu (red line) and 58.043 ± 0.003 amu (purple line) consistent with the mass of glyoxal/ α -lactone (58.005 amu) and C_3H_6O (58.042 amu), respectively. A PIE curve is associated with the lower mass region (57.95-58.00) is shown in the upper panel of Figure 4. The resultant PIE curve matches the onset (ca. 10.2 eV) and shape of the previously measured PI spectrum of glyoxal (black line).⁵⁵ No evidence of α -lactone is discernable in the PIE curve, consistent with the low yield of stabilization previously reported.^{28, 35-37, 39-40, 42}

B. MACR-oxide

Acetaldehyde (m/z 44), methylketene (m/z 56), and acrolein (m/z 56) are anticipated to be final products generated from the unimolecular decay of *syn*-MACR-oxide via the dioxole pathway and subsequent reaction of the radical products with O_2 (Section II, Schemes 8 and 9). The fast appearance of signal on the m/z 44 channel is consistent with rapid product formation, as shown in the temporal profile of m/z 44 (9.0-11.0 eV) in the top panel of Figure 5. The photoionization signal is constant at long reaction times indicating a stable spectral carrier. A high-resolution mass spectrum of m/z 44 is shown in the inset of Figure 5. A Gaussian fit to the feature yields a single peak at 44.028 ± 0.003 , in accord with the chemical composition of acetaldehyde (CH_3CHCO , 44.026). Figure 5 (bottom) shows the PIE curve of m/z 44 integrated over the full kinetic time window (open circles, 0-80 ms), which reveals low and high energy components indicative of multiple species contributing to the photoionization signal.

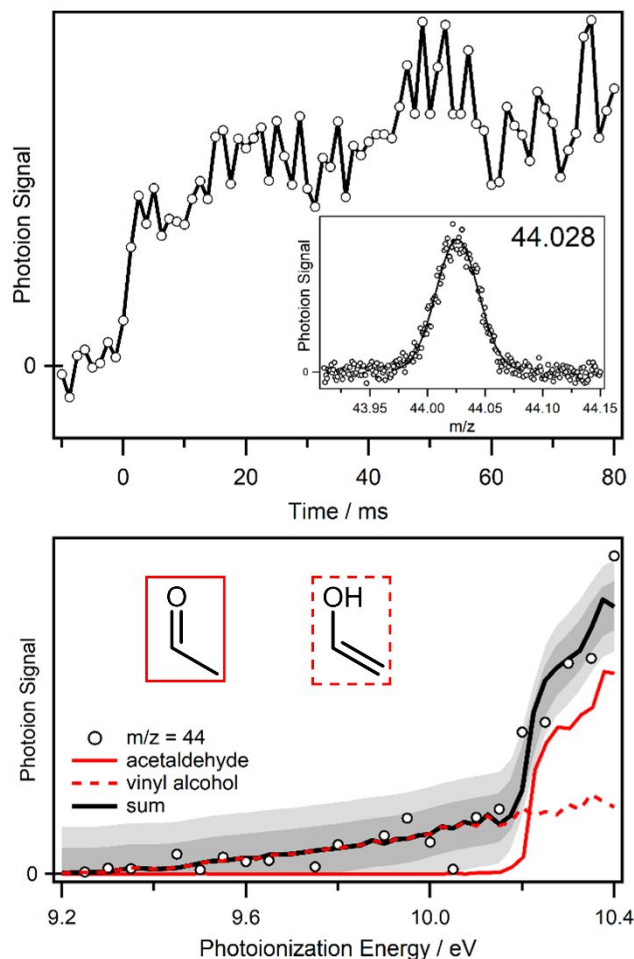


Figure 5. (Top, inset) High-resolution mass spectrum of the m/z 44 signal integrated over the full kinetic time window (0-80 ms) and photoionization energies (9.0-10.7 eV). (Top) Temporal profile of the m/z 44 over the 9.0-10.7 eV photoionization energy range. (Bottom) PIE curve of m/z 44 (open circles) integrated over the full kinetic time window (0-80 ms). The onset and shape of the spectrum at lower energies is consistent with the absolute photoionization spectrum of vinyl alcohol (red dashed line).⁵⁷ At higher energies (ca. 10.2 eV) a higher intensity feature is observed that is consistent with the absolute photoionization spectrum of acetaldehyde (red solid line).⁵⁸ The black line results from a least squares fit of the absolute photoionization spectra to the experimental $m/z = 44$ data. The darker and lighter grey shaded regions represent 1σ and 2σ uncertainty in the fit, respectively

Since only a single peak is observed in the high-resolution mass spectrum (44.028 amu), the species contributing to the PIE spectrum must have the same chemical composition and therefore are isomers. The onset (ca. 10.2 eV)⁵⁹ and shape of the higher energy component is consistent with the absolute photoionization spectrum of acetaldehyde (red solid line),⁵⁸ confirming its formation. The appearance energy (ca. 9.3 eV) and shape of the lower intensity feature agrees well with the absolute photoionization spectrum of vinyl alcohol (red dashed line).⁵⁷ Vinyl alcohol is likely generated directly from the

1
2
3 exothermic unimolecular decay of QOOH-4 as the barrier for isomerization of acetaldehyde to vinyl
4 alcohol is large (ca. 70 kcal mol⁻¹).⁶⁰ The experimental PIE curve is fit to the absolute spectra of
5 acetaldehyde and vinyl alcohol by a least squares method and the resultant fit is shown in Figure 5 (black
6 line). Uncertainty in the fit ($\pm \sigma$, $\pm 2\sigma$) is indicated by the shaded regions.
7
8
9

10
11 Rapid product formation is also observed on the m/z 56 mass channel. The temporal profile persists to
12 long reaction times although it shows a slow decay after formation likely due to secondary chemistry
13 (9.0-11.0 eV, Figure 6, top panel). A high-resolution mass spectrum of m/z 56 is shown in the inset of the
14 top panel of Figure 6. A Gaussian fit to the feature results in a peak center of 56.029 ± 0.003 , which is
15 consistent with the chemical composition of methylketene and acrolein (C₃H₄O, 56.026 amu). The
16 corresponding PIE curve integrated over the full kinetic time window (0-80 ms) is shown in Figure 6
17 (bottom panel).
18
19
20
21
22
23
24
25

26 Two components are apparent in the PIE curve: a lower intensity component at low photoionization
27 energies and a higher intensity component at high photoionization energies. The lower intensity
28 component and higher intensity component matches the onset and shape of the absolute PI spectra of
29 methylketene (9.0 eV, blue dashed line)⁵⁵ and acrolein (10.1 eV, blue solid line),^{58, 61} respectively. The
30 experimental data is fit to a sum of the methylketene and acrolein absolute photoionization spectra via a
31 least squares method (black line). Uncertainty in the fit ($\pm \sigma$, $\pm 2\sigma$) is indicated by the shaded regions.
32
33
34
35
36
37
38
39
40
41
42
43
44
45
46
47
48
49
50
51
52
53
54
55
56
57
58
59
60

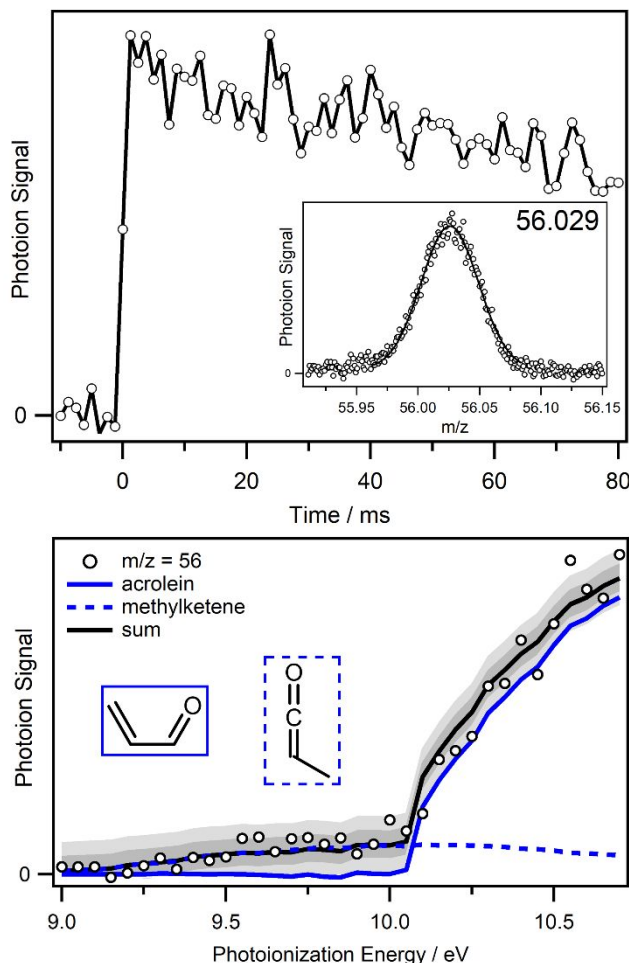


Figure 6. (Top, inset) High-resolution mass spectrum of the m/z 56 signal integrated over the full kinetic time window (0-80 ms) and photoionization energies (9.0-10.7 eV). (Top) Temporal profile of the m/z 56 over the 9.0-10.7 eV photoionization energy range. (Bottom) PIE curve of m/z 56 (open circles) integrated over the full kinetic time window (0-80 ms). The appearance energy of the photoionization spectrum is consistent with the absolute photoionization spectrum of methylketene alcohol (blue dashed line). At higher energies (ca. 10.1 eV) a higher intensity feature is observed that is consistent with the absolute spectrum of acrolein (blue solid line). The black line shows the result of a least squares fit of the absolute photoionization spectra of acrolein and methylketene to the experimental m/z 56 data. The darker and lighter grey shaded regions represent 1σ and 2σ uncertainty in the fit, respectively.

Discussion

A. Product Yields

High level *ab initio* calculations show that the unimolecular decay of the *anti*-MVK-oxide Criegee intermediate via the dioxole channel results in the generation of acetyl and vinyloxy radical products.¹⁵ An analogous pathway is predicted for *syn*-MACR-oxide leading to formyl and 2-methyl-vinyloxy radical

products. Previous experimental and theoretical studies indicate that under the present experimental conditions, the radical products will rapidly undergo O_2 addition to generate ROO.²⁸⁻³⁰ These ROO are predicted to decay to closed shell products (Section II), which are identified using MPIMS (Section IV), along with transient OH or HO_2 radical co-products.

A quantitative analysis is conducted to determine the relative yields of the product channels identified from unimolecular decay of *anti*-MVK-oxide and *syn*-MACR-oxide to radical products, and subsequent ROO chemistry. The known absolute photoionization spectra of the products are scaled to fit the experimental PIE curves via a least squares method.^{53, 55, 57-58, 62} The resultant scaling factors correspond to the relative observed abundance of each product channel. Uncertainties in the fits, and ultimately the relative product yields, are obtained by propagating the error associated with the least squares fitting method. Additional details of the analysis are provided in the Supporting Information (SI Sec. S2, Figures S1-S3).

For the unimolecular decay of *anti*-MVK-oxide via the dioxole channel and subsequent ROO chemistry, formaldehyde, ketene and glyoxal are identified as principal products. The results from the product analysis indicate that formaldehyde + OH + CO is the dominant product channel ($88\% \pm 5\%$) with ketene + HO_2 and glyoxal + OH as minor product channels ($9\% \pm 1\%$ and $3\% \pm 1\%$, respectively). The resultant trend in product yields agrees well with theoretical predictions for the acetyl radical + O_2 and vinoxy radical + O_2 reactions.²⁸⁻²⁹

For the unimolecular decay of *syn*-MACR-oxide via the dioxole channel and subsequent reaction of 2-methyl-vinoxy radical product with O_2 , acetaldehyde, vinyl alcohol, methylketene, and acrolein products are identified as main products (Figure 5 and 6). The minimum energy pathway predicted theoretically leads to acetaldehyde + CO + OH products. The total branching to this product channel, including the formation of vinyl alcohol ($9\% \pm 1\%$) is $46\% \pm 7\%$. Methylketene + HO_2 is found to be a minor product channel ($2\% \pm 1\%$), while acrolein + HO_2 is found to be the principal product channel ($52\% \pm 5\%$). This is the most direct route to products as acrolein + HO_2 is generated directly from the 1-oxo-2-propylperoxy radical (Scheme 9) and does not proceed through the QOOH-4 intermediate. Master

equation modeling of the 2-methyl-vinoy + O₂ reaction (Section C) indicates the acrolein product channel will not have an appreciable yield due to the high barrier (Scheme 9, 27.4 kcal mol⁻¹) for its formation. This suggests there may be a lower barrier pathway to acrolein + HO₂ products that has not been identified or an additional source of acrolein in the experiment. In the latter case, acetaldehyde + CO + OH would be the dominant product channel (ca. 96%).

B. Scavenger experiments

Additional experiments were conducted to robustly determine whether the stable products observed are generated from the dioxole pathway followed by reaction with O₂. These studies were conducted for the MVK-oxide Criegee intermediate only, for which the reaction rate coefficient with formic acid has recently been determined.¹⁶ Formic acid was introduced into the flow cell at sufficient concentration for its bimolecular reaction rate with MVK-oxide to surpass the predicted thermal decay rate for *anti*-MVK-oxide (2140 s⁻¹, 298 K, 760 torr). As a result, *anti*-MVK-oxide will react more quickly with formic acid than undergo unimolecular decay, resulting in a decrease in the product yields from the dioxole pathway. We assume that *anti*-MVK-oxide reacts with formic acid at a similar rate to *syn*-MVK-oxide and alkyl-substituted Criegee intermediates (ca. 10⁻¹⁰ cm³ s⁻¹).^{16, 63}

Figure 7 shows temporal profiles of the m/z 30 channel (formaldehyde) measured using a photoionization energy of 11.0 eV. The temporal profile shows prompt formation of m/z 30 followed by a slow growth in signal. Upon introduction of formic acid, the m/z 30 signal is significantly reduced, leaving a prompt signal that persists to long kinetic time.

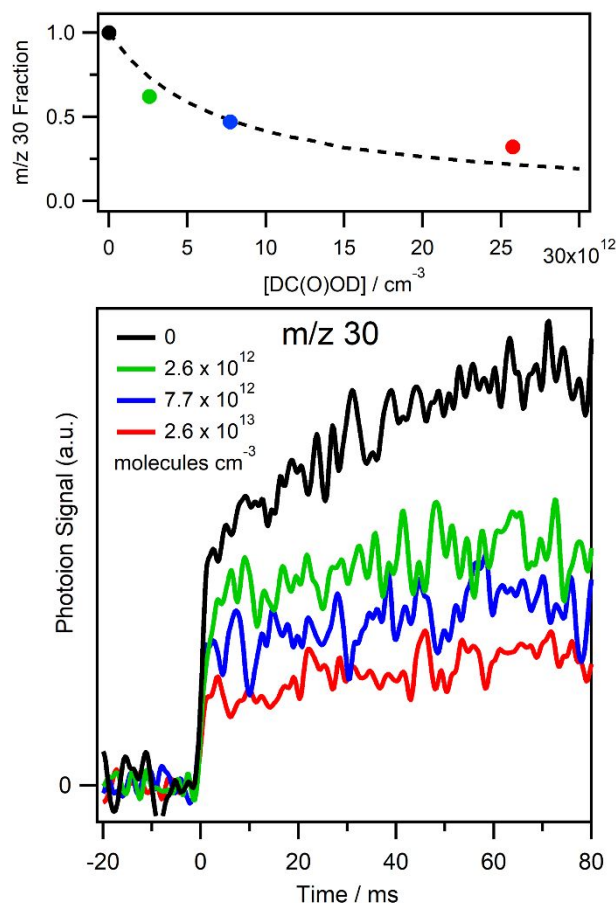


Figure 7. (Bottom) Temporal profiles of m/z 30 (11.0 eV) measured at varying formic acid concentrations. (Top) Fraction of m/z 30 signal remaining versus formic acid concentration compared to a kinetic model (dashed line).

The fraction of the m/z 30 signal remaining upon introduction of formic acid at specific concentrations is shown in the top panel of Figure 7 (solid circles). This is obtained by normalizing the integrated m/z 30 signal by the integrated I-atom (m/z 127) signal to account for experimental fluctuations, e.g. laser power or precursor concentration. Further, the integrated m/z 30 signal recorded in the absence of formic acid is set to 1 (black solid circle). A simple model is used to predict the fraction f of m/z 30 that would remain with increasing formic acid concentration (dashed line, top panel) according to equation (1):

$$(1) \quad f = \frac{r_{uni}}{r_{uni} + r_{acid}}$$

Here, r_{uni} is the thermal decay rate for *anti*-MVK-oxide (2140 s⁻¹)¹⁵ and r_{acid} is the effective rate of reaction between *anti*-MVK-oxide and formic acid at a specific concentration. The model assumes that

m/z 30 arises solely from unimolecular decay of *anti*-MVK-oxide to radical products and subsequent peroxy radical chemistry, the thermal decay rate (298 K) of *anti*-MVK-oxide is 2140 s^{-1} , and the rate constant for the reaction of *anti*-MVK-oxide with formic acid is the same as that for *syn*-MVK-oxide ($3.0 \times 10^{-10} \text{ cm}^3 \text{ s}^{-1}$). The results obtained agree reasonably well with the simple model.

There may be an additional source of formaldehyde that gives rise to the slow growth in signal on the m/z 30 channel. One possibility is that secondary chemistry associated with products from unimolecular decay of *syn*-MVK-oxide may produce formaldehyde. However, even at the lowest formic acid concentration used in the experiment ($2.6 \times 10^{12} \text{ molecules cm}^{-3}$, green), more than 95% of *syn*-MVK-oxide is expected to undergo bimolecular reaction with acid rather than unimolecular decay.

If there is another source of formaldehyde, the product yield to the formaldehyde + OH + CO channel would be overestimated. For example, if 50% of the m/z 30 signal is from a different source, the formaldehyde + OH + CO channel will be less dominant, but still the major product channel ($79 \pm 3\%$), while the ketene + HO₂ and glyoxal + OH product channels would become more significant ($16 \pm 1\%$ and $5 \pm 1\%$, respectively). Unfortunately, addition of formic acid results in formation of a daughter ion at energies above the ionization energy of ketene on the m/z 42 mass channel that precludes scavenger studies of the ketene product channel.

C. Atmospheric implications

Rapid unimolecular decay of *anti*-MVK-oxide and *syn*-MACR-oxide to dioxole (2150 and 2500 s^{-1} , respectively; 298 K, 760 torr)^{15, 17} and subsequent formation of radical products is expected to be the dominant sink for these Criegee intermediates under atmospheric conditions.¹⁶ Under our low pressure experimental conditions (298 K, 10 torr), the radical products react with O₂ to form ROO, which undergoes further unimolecular decay via QOOH intermediates to yield stable carbonyl products that are detected and an OH or HO₂ radical co-product.²⁷⁻³⁰ The radical products are expected to have a similar fate under atmospheric conditions (298 K, 760 torr) in pristine locations (low NO_x concentrations).⁶⁴⁻⁶⁵ Again, the radicals will react rapidly with O₂ to form ROO, which can undergo unimolecular decay to stable carbonyl products with an OH or HO₂ radical co-product. Alternatively, the ROO can be

collisionally stabilized and thermally decay on a longer timescale (minutes), and/or undergo bimolecular reactions.⁶⁶⁻⁶⁷

Previous experiment and theory has shown that the acetyl radical + O₂ reaction exhibits a significant pressure dependence.²⁸ The OH yield drops from near unity at low pressure to ~4% at atmospheric pressure as a result of collisional stabilization of ROO at higher pressures.²⁸ A similar pressure dependence has been predicted theoretically by Kuwata *et al.*⁶⁸ for the vinoxy and 2-methyl-vinoxy + O₂ reactions, resulting in OH yields at atmospheric pressure of 25% and 5%, respectively.⁶⁸ More recent high-level electronic structure calculations by Weidman *et al.*²⁹ and Davis *et al.*³⁰ predict higher barriers for ROO dissociation back to reactants (vinoxy radical + O₂) than earlier calculations⁶⁸ and similar barriers for H-atom transfer leading to the QOOH intermediates. The higher barriers suggest that the previously computed OH yields⁶⁸ for these reactions may be overestimated. Therefore, we carried out master equation simulations (MESMER, SI Sec. S3)⁶⁹ to reinvestigate the OH yields from these reactions under atmospheric conditions. We find that the higher barriers^{29,30} result in lower OH yields from the vinoxy + O₂ (5%) and 2-methyl-vinoxy + O₂ (2%) reactions under atmospheric conditions (298 K, 760 torr).

Given the large abundance of isoprene emitted into the atmosphere, we wanted to assess the potential atmospheric yield of OH radicals arising from the dioxole pathway and subsequent reaction of its radical products with O₂. Specifically, we estimate the OH yield derived from unimolecular decay of *anti*-MVK-oxide and *syn*-MACR-oxide, and subsequent peroxy radical chemistry under atmospheric conditions. This is then compared to the total OH yield from isoprene ozonolysis. The OH yield from isoprene ozonolysis has been reported from a variety of indirect methods that include the use of OH scavengers and tracers such as methylcyclohexane,⁷⁰ cyclohexane,⁷¹⁻⁷⁴ CO,⁷⁵⁻⁷⁶ trimethylbenzene,^{74, 77-78} as well as a limited number of direct OH measurements by laser-induced fluorescence,^{74, 79} and a comprehensive model that used experimental measurements as constraints in determining the OH yield.² The reported OH yields vary considerably (19% to 68%). Here, we compare to the IUPAC recommended OH yield from isoprene ozonolysis of 25%.⁸⁰

The OH yield from the dioxole pathway and subsequent peroxy radical chemistry is estimated by combining the yields of MVK-oxide and MACR-oxide from isoprene ozonolysis (23% and 19%, respectively),² the predicted reactive fluxes through the dioxole channel (42% and 25%, respectively),¹⁸⁻¹⁹ and the predicted OH yields from the respective radical + O₂ reactions under atmospheric conditions (see above). The resultant OH yield accounts for only ca. 4% of the total OH radicals produced from isoprene ozonolysis under atmospheric conditions. This estimate assumes that the radicals generated from the exothermic dioxole pathway are fully thermalized prior to reaction with O₂ and formation of ROO. If ROO is formed internally excited, the estimated OH yield from the dioxole pathway may be underestimated. Thus, we conclude that dominant source of OH radicals from isoprene ozonolysis under atmospheric conditions is thermal unimolecular decay of *syn*-MVK-oxide via a 1,4 H-atom transfer mechanism (33 s⁻¹ at 298 K, 760 torr).^{2, 15, 17}

Current atmospheric models utilizing the Master Chemical Mechanism (MCM)⁸¹ for tropospheric degradation of primary emitted volatile organic compounds indicate that decomposition of Criegee intermediates derived from isoprene ozonolysis is a substantial source of OH radicals, even when compared to all atmospheric sources of OH production. The OH production is predicted to be greatest over heavily forested regions including the Amazon, in particular at nighttime.⁷ The present work on the dioxole unimolecular pathway and subsequent bimolecular reactions of the radicals produced with molecular oxygen may extend the possible sources of atmospheric OH radicals. While the stabilization and bimolecular reactions of ROO with NO_x, HO₂ and other RO₂ are included in the current MCM, the unimolecular decay processes discussed in this work are not. Future work will assess if inclusion of these reaction mechanisms significantly impacts the generation of OH radicals from isoprene ozonolysis.

In addition, the production of ketene and methyl ketene may be substantial from ozonolysis of isoprene, and are estimated to be on the order of 2 Gg and 0.5 Gg, respectively. Given a rough estimate for the atmospheric lifetime of ketene (e.g. 5-15 hours) and its rate of reaction with OH (ca. 10⁻¹¹ cm³ molecule⁻¹ s⁻¹),⁸² we anticipate that ketene and methylketene will be elevated close to the emission source of isoprene. Thus, ketene emission is a potential marker for ozonolysis of isoprene and other dialkenes,

including acyclic monoterpenes, ocimene, and myrcene. In addition, ketene has a well-defined IR absorption spectrum and can be a useful tracer in chamber studies.⁸³

Conclusions

MVK-oxide and MACR-oxide, the four-carbon unsaturated Criegee intermediates generated in isoprene ozonolysis, have been photolytically generated in a flow cell (298 K, 10 torr) in the presence of O₂. Specific conformational forms of MVK-oxide (*anti*) and MACR-oxide (*syn*) with the vinyl substituent adjacent to the terminal O atom can rapidly isomerize via an exothermic electrocyclic ring closure mechanism to form a 5-membered cyclic peroxide, known as dioxole.^{15, 17-19} Dioxole is formed with sufficient internal excitation to undergo rapid unimolecular decay to oxygenated hydrocarbon radicals, producing acetyl and vinoxy radicals from MVK-oxide and formyl and 2-methyl-vinoxy radicals from MACR-oxide. In the presence of O₂ under our laboratory conditions, the newly formed radicals quickly react with O₂ in a barrierless, exothermic reaction that yields peroxy radicals.²⁷⁻³⁰ The peroxy radicals undergo H-atom transfer to form QOOH intermediates, which decay via submerged barriers to form closed shell carbonyl species.²⁸⁻³⁰ The resultant stable carbonyl products are detected by MPIMS, providing the first experimental evidence of the dioxole unimolecular decay pathway for the four-carbon unsaturated Criegee intermediates from isoprene ozonolysis. The main products identified in the unimolecular decay of *anti*-MVK-oxide and subsequent reaction of acetyl and vinoxy radicals with O₂ are formaldehyde (88 ± 5%), ketene (9 ± 1%) and glyoxal (3 ± 1%). Those identified from the unimolecular decay of *syn*-MACR-oxide and subsequent reaction of 2-methyl-vinoxy radicals with O₂ are acetaldehyde (37 ± 7%), vinyl alcohol (9 ± 1%), methylketene (2 ± 1%), and acrolein (52 ± 6%). In separate experiments, sufficient formic acid is added to ensure that its bimolecular reaction with *anti*-MVK-oxide competes with unimolecular decay, thereby reducing the yield of products arising from unimolecular decay and subsequent reaction with O₂. Bimolecular reaction with formic acid is shown to decrease the yield of formaldehyde products arising from unimolecular decay of MVK-oxide. In addition to the stable

carbonyl products that are observed, the peroxy chemistry also results in OH or HO₂ radical co-products with pressure-dependent yields.

Supporting Information

Supporting information includes computed stationary point geometries and zero point corrected energies, detailed description of the product branching analysis, and MESMER input files.

Acknowledgements

This research was supported by the U.S. Department of Energy-Basic Energy Sciences under grant DE-FG02-87ER13792 (MIL). This material is also based upon work supported by the Division of Chemical Sciences, Geosciences and Biosciences, Office of Basic Energy Sciences (BES), U.S. Department of Energy (USDOE). Sandia National Laboratories is a multimission laboratory managed and operated by National Technology and Engineering Solutions of Sandia, LLC., a wholly owned subsidiary of Honeywell International, Inc., for the USDOE's National Nuclear Security Administration under contract DE-NA0003525. This paper describes objective technical results and analysis. Any subjective views or opinions that might be expressed in the paper do not necessarily represent the views of the USDOE or the United States Government. This material is based in part on research at Argonne supported by the U.S. Department of Energy, Office of Science, Office of Basic Energy Sciences, Division of Chemical Sciences, Geosciences, and Biosciences under Contract No. DE-AC02-06CH11357. The Advanced Light Source is supported by the Director, Office of Science, BES/USDOE under Contract DE-AC02-05CH11231 at Lawrence Berkeley National Laboratory. This research was carried out in part by the Jet Propulsion Laboratory, California Institute of Technology, under contract with the National Aeronautics and Space Administration (NASA), supported by the Upper Atmosphere Research and Tropospheric Chemistry program. The contributions of RLC and KLZ were in part supported by appointments to the NASA Postdoctoral Program at the NASA Jet Propulsion Laboratory, administered by Universities Space Research Association under contract with NASA. PJW thanks the NSF (CHE-1902509). DES and MAHK thank NERC (grant codes-NE/K004905/1), Bristol ChemLabS and Primary Science Teaching Trust under whose auspices various aspects of this work was funded. California Institute of Technology. © 2019. All rights reserved.

References

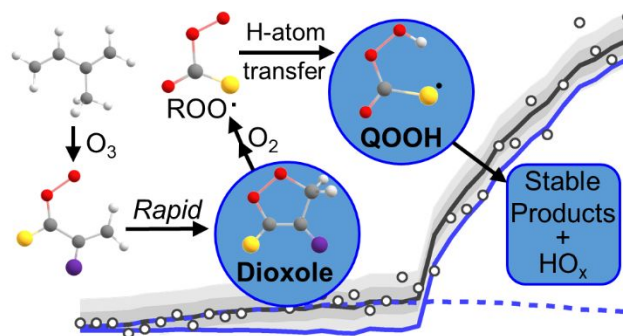
1. Sindelarova, K.; Granier, C.; Bouarar, I.; Guenther, A.; Tilmes, S.; Stavrakou, T.; Müller, J. F.; Kuhn, U.; Stefani, P.; Knorr, W. Global Data Set of Biogenic VOC Emissions calculated by the MEGAN Model Over the Last 30 years. *Atmos. Chem. Phys.* **2014**, *14*, 9317-9341.
2. Nguyen, T. B.; Tyndall, G. S.; Crounse, J. D.; Teng, A. P.; Bates, K. H.; Schwantes, R. H.; Coggon, M. M.; Zhang, L.; Feiner, P.; Milller, D. O., et al. Atmospheric fates of Criegee intermediates in the ozonolysis of isoprene. *Phys. Chem. Chem. Phys.* **2016**, *18*, 10241-10254.
3. Finlayson-Pitts, B. J.; Pitts, J. N., *Chemistry of the Upper and Lower Atmosphere*. Academic Press: San Diego, 2000.
4. Lester, M. I.; Klippenstein, S. J. Unimolecular Decay of Criegee Intermediates to OH Radical Products: Prompt and Thermal Decay Processes. *Acc. Chem. Res.* **2018**, *51*, 978-985.
5. Emmerson, K. M.; Carslaw, N.; Carslaw, D. C.; Lee, J. D.; McFiggans, G.; Bloss, W. J.; Gravestock, T.; Heard, D. E.; Hopkins, J.; Ingham, T., et al. Free radical modelling studies during the UK TORCH Campaign in Summer 2003. *Atmos. Chem. Phys.* **2007**, *7*, 167-181.
6. Emmerson, K. M.; Carslaw, N. Night-time radical chemistry during the TORCH campaign. *Atmos. Environ.* **2009**, *43*, 3220-3226.
7. Khan, M. A. H.; Percival, C. J.; Caravan, R. L.; Taatjes, C. A.; Shallcross, D. E. Criegee intermediates and their impacts on the troposphere. *Environ. Sci.: Process. Impacts* **2018**, *20*, 437-453.
8. Vansco, M. F.; Marchetti, B.; Lester, M. I. Electronic spectroscopy of methyl vinyl ketone oxide: A four-carbon unsaturated Criegee intermediate from isoprene ozonolysis. *J. Chem. Phys.* **2018**, *149*, 244309.
9. Vansco, M. F.; Marchetti, B.; Trongsirawat, N.; Wang, G.; Bhagde, T.; Walsh, P. J.; Klippenstein, S. J.; Lester, M. I. Synthesis, electronic spectroscopy and photochemistry of methacrolein oxide: A four carbon unsaturated Criegee intermediate from isoprene ozonolysis. *J. Am. Chem. Soc.* **2019**, *141*, 15058-15069.
10. Welz, O.; Savee, J. D.; Osborn, D. L.; Vasu, S. S.; Percival, C. J.; Shallcross, D. E.; Taatjes, C. A. Direct Kinetic Measurements of Criegee Intermediate (CH_2OO) Formed by Reaction of CH_2I with O_2 . *Science* **2012**, *335*, 204-207.
11. Beames, J. M.; Liu, F.; Lu, L.; Lester, M. I. Ultraviolet Spectrum and Photochemistry of the Simplest Criegee Intermediate CH_2OO . *J. Am. Chem. Soc.* **2012**, *134*, 20045-20048.
12. Taatjes, C. A.; Welz, O.; Eskola, A. J.; Savee, J. D.; Scheer, A. M.; Shallcross, D. E.; Rotavera, B.; Lee, E. P. F.; Dyke, J. M.; Mok, D. K. W., et al. Direct Measurements of Conformer-Dependent Reactivity of the Criegee Intermediate CH_3CHOO . *Science* **2013**, *340*, 177-180.
13. Beames, J. M.; Liu, F.; Lu, L.; Lester, M. I. UV spectroscopic characterization of an alkyl substituted Criegee intermediate CH_3CHOO . *J. Chem. Phys.* **2013**, *138*, 244307.
14. Liu, F.; Beames, J. M.; Green, A. M.; Lester, M. I. UV Spectroscopic Characterization of Dimethyl- and Ethyl-Substituted Carbonyl Oxides. *J. Phys. Chem. A* **2014**, *118*, 2298-2306.
15. Barber, V. P.; Pandit, S.; Green, A. M.; Trongsirawat, N.; Walsh, P. J.; Klippenstein, S. J.; Lester, M. I. Four-Carbon Criegee Intermediate from Isoprene Ozonolysis: Methyl Vinyl Ketone Oxide Synthesis, Infrared Spectrum, and OH Production. *J. Am. Chem. Soc.* **2018**, *140*, 10866-10880.
16. Caravan, R. L.; Vansco, M. F.; Au, K.; Khan, M. A. H.; Li, Y.-L.; Winiberg, F. A. F.; Zuraski, K.; Lin, Y.-H.; Chao, W.; Trongsirawat, N., et al. First direct kinetic measurements and theoretical predictions of an isoprene-derived Criegee intermediate. *Proc. Natl. Acad. Sci.* **2020**, in press.
17. Vereecken, L.; Novelli, A.; Taraborrelli, D. Unimolecular decay strongly limits the atmospheric impact of Criegee intermediates. *Phys. Chem. Chem. Phys.* **2017**, *19*, 31599-31612.
18. Kuwata, K. T.; Valin, L. C.; Converse, A. D. Quantum Chemical and Master Equation Studies of the Methyl Vinyl Carbonyl Oxides Formed in Isoprene Ozonolysis. *J. Phys. Chem. A* **2005**, *109*, 10725.
19. Kuwata, K. T.; Valin, L. C. Quantum Chemical and RRKM/Master Equation Studies of Isoprene Ozonolysis: Methacrolein and Methacrolein Oxide. *Chem. Phys. Lett.* **2008**, *451*, 186-191.

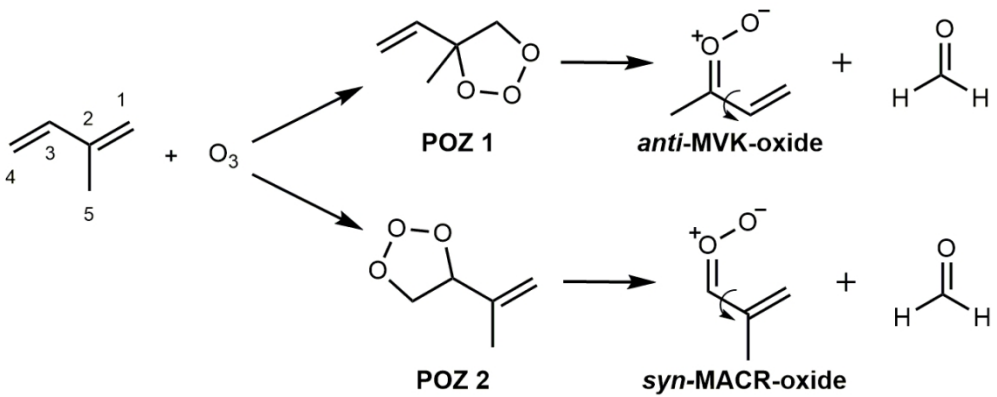
20. Zhang, D.; Lei, W.; Zhang, R. Mechanism of OH formation from ozonolysis of isoprene: kinetics and product yields. *Chem. Phys. Lett.* **2002**, *358*, 171–179.
21. Stephenson, T. A.; Lester, M. I. Unimolecular decay dynamics of Criegee intermediates: Energy-resolved rates, thermal rates, and their atmospheric impact. *Int. Rev. Phys. Chem.* **2020**, *39*, 1–33.
22. Anglada, J. M.; Solé, A. Impact of the water dimer on the atmospheric reactivity of carbonyl oxides. *Phys. Chem. Chem. Phys.* **2016**, *18*, 17698–17712.
23. Welz, O.; Eskola, A. J.; Sheps, L.; Rotavera, B.; Savee, J. D.; Scheer, A. M.; Osborn, D. L.; Lowe, D.; Murray Booth, A.; Xiao, P., et al. Rate Coefficients of C1 and C2 Criegee Intermediate Reactions with Formic and Acetic Acid Near the Collision Limit: Direct Kinetics Measurements and Atmospheric Implications. *Angew. Chem. Int. Ed.* **2014**, *53*, 4547–4550.
24. Chhantyal-Pun, R.; Davey, A.; Shallcross, D. E.; Percival, C. J.; Orr-Ewing, A. J. A kinetic study of the CH₂OO Criegee intermediate self-reaction, reaction with SO₂ and unimolecular reaction using cavity ring-down spectroscopy. *Phys. Chem. Chem. Phys.* **2015**, *17*, 3617–3626.
25. Vereecken, L.; Harder, H.; Novelli, A. The reaction of Criegee intermediates with NO, RO₂, and SO₂, and their fate in the atmosphere. *Phys. Chem. Chem. Phys.* **2012**, *14*, 14682–14695.
26. Vereecken, L. The reaction of Criegee intermediates with acids and enols. *Phys. Chem. Chem. Phys.* **2017**, *19*, 28630–28640.
27. Martínez-Ávila, M.; Peiró-García, J.; Ramírez-Ramírez, V. M.; Ignacio, N.-G. Ab initio study on the mechanism of the HCO + O₂ → HO₂ + CO reaction. *Chem. Phys. Lett.* **2003**, *370*, 313–318.
28. Carr, S. A.; Glowacki, D. R.; Liang, C.-H.; Baeza-Romero, M. T.; Blitz, M. A.; Pilling, M. J.; Seakins, P. W. Experimental and Modeling Studies of the Pressure and Temperature Dependences of the Kinetics and the OH Yields in the Acetyl + O₂ Reaction. *J. Phys. Chem A* **2011**, *115*, 1069–1085.
29. Weidman, J. D.; Allen, R. T.; Moore III, K. B.; Schaefer III, H. F. High-level theoretical characterization of the vinoxy radical (•CH₂CHO) + O₂ reaction. *J. Chem. Phys.* **2018**, *148*, 184308.
30. Davis, M. M.; Weidman, J. D.; Abbott, A. S.; Douberly, G. E.; Turney, J. M.; Schaefer III, H. F. Characterization of the 2-methylvinoxy radical + O₂ reaction: A focal point analysis and composite multireference study. *J. Chem. Phys.* **2019**, *151*, 124302.
31. Gleason, J. F.; Stief, L. J. Temperature Dependence of the Rate Constant for the Reaction HCO + O₂ → HO₂ + CO at T = 200–398 K. *J. Phys. Chem. A* **1999**, *103*, 3038–3043.
32. Ninomiya, Y.; Goto, M.; Hashimoto, S.; Kagawa, Y.; Yoshizawa, K.; Kawasaki, M. Cavity Ring-Down Spectroscopy and Relative Rate Study of Reactions of HCO Radicals with O₂, NO, NO₂, and Cl₂ at 295 K. *J. Phys. Chem. A* **2000**, *104*, 7556–7564.
33. Hanoune, B.; Dusanter, S.; ElMaimouni, L.; Devolder, P.; Lemoine, B. Rate constant determinations by laser photolysis/diode laser infrared absorption: examples of HCO + O₂ → HCH(O) + HO₂ reactions at 294 K. *Chem. Phys. Lett.* **2001**, *343*, 527–534.
34. Michael, J. V.; Keil, D. G.; Klemm, R. B. Rate constants for the reaction of hydroxyl radicals with acetaldehyde from 244–528 K. *J. Chem. Phys.* **1985**, *83*, 1630.
35. Tyndall, G. S.; Orlando, J. J.; Wallington, T. J.; Hurley, M. D. Pressure dependence of the rate coefficients and product yields for the reaction of CH₃CO radicals with O₂. *Int. J. Chem. Kinet.* **1997**, *29*, 655–663.
36. Blitz, M. A.; Heard, D. E.; Pilling, M. J. OH formation from CH₃CO + O₂: a convenient experimental marker for the acetyl radical. *Chem. Phys. Lett.* **2002**, *365*, 374–379.
37. Hou, H.; Li, A.; Hu, H.; Li, Y.; Li, H.; Wang, B. Mechanistic and kinetic study of the CH₃CO + O₂ reaction. *J. Chem. Phys.* **2005**, *122*, 224304.
38. Devolder, P.; Dusanter, S.; Lemoine, B.; Fittschen, C. About the co-product of the OH radical in the reaction of acetyl with O₂ below atmospheric pressure. *Chem. Phys. Lett.* **2006**, *417*, 154–158.
39. Kovács, G.; Zádor, J.; Farkas, E.; Nádasdi, R.; Szilágyi, I.; Dóbbé, S.; Bérces, T.; Márta, F.; Lendvay, G. Kinetics and mechanism of the reactions of CH₃CO and CH₃C(O)CH₂ radicals with O₂. Low-pressure discharge flow experiments and quantum chemical computations. *Phys. Chem. Chem. Phys.* **2007**, *9*, 4142–4154.

40. Carr, S. A.; Baeza-Romero, M. T.; Blitz, M. A.; Pilling, M. J.; Heard, D. E.; Seakins, P. W. OH yields from the $\text{CH}_3\text{CO} + \text{O}_2$ reaction using an internal standard. *Chem. Phys. Lett.* **2007**, *445*, 108-112.
41. Maranzana, A.; Barker, J. R.; Tonachini, G. Master equation simulations of competing unimolecular and bimolecular reactions: application to OH production in the reaction of acetyl radical with O_2 . *Phys. Chem. Chem. Phys.* **2007**, *9*, 4129-4141.
42. Chen, S.-Y.; Lee, Y.-P. Transient infrared absorption of *t*- $\text{CH}_3\text{C}(\text{O})\text{OO}$, *c*- $\text{CH}_3\text{C}(\text{O})\text{OO}$, and α -lactone recorded in gaseous of CH_3CO and O_2 . *J. Chem. Phys.* **2010**, *132*, 114303.
43. Seakins, P. W.; Blitz, M. A. Developments in Laboratory Studies of Gas-Phase Reactions for Atmospheric Chemistry with Applications to Isoprene Oxidation and Carbonyl Chemistry. *Annu. Rev. Phys. Chem.* **2011**, *62*, 351-373.
44. Inoue, G.; Akimoto, H. Laser-induced fluorescence of the $\text{C}_2\text{H}_3\text{O}$ radical. *J. Chem. Phys.* **1981**, *74*, 425-433.
45. Dupuis, M.; Wendoloski, J. J.; Lester, W. A. J. Electronic structure of vinoxy radical CH_2CHO . *J. Chem. Phys.* **1982**, *76*, 488-492.
46. Jacox, M. E. The reaction of F atoms with acetaldehyde and ethylene oxide. Vibrational spectra of the CH_3CO and CH_2CHO free radicals trapped in solid argon. *Chem. Phys.* **1982**, *69*, 407-422.
47. Oguchi, T.; Miyoshi, A.; Koshi, M.; Matsui, H.; Washida, N. Kinetic Study on Reactions of 1- and 2-Methylvinoxy Radicals with O_2 . *J. Phys. Chem. A* **2001**, *105*, 378-382.
48. Delbos, E.; Fittschen, C.; Hippler, H.; Krasteva, N.; Olzmann, M.; Viskolcz, B. Rate Coefficients and Equilibrium Constant for the $\text{CH}_2\text{CHO} + \text{O}_2$ Reaction System. *J. Phys. Chem. A* **2006**, *110*, 3238-3245.
49. Zhu, L.; Johnston, G. Kinetics and Products of the Reaction of the Vinyloxy Radical with O_2 . *J. Phys. Chem.* **1995**, *99*, 15114-15119.
50. Si-Ok, R.; Shin, K. S.; Hwang, S. M. Determination of the Rate Coefficients of the $\text{CH}_4 + \text{O}_2 \rightarrow \text{HO}_2 + \text{CH}_3$ and $\text{HCO} + \text{O}_2 \rightarrow \text{HO}_2 + \text{CO}$ Reactions at High Temperatures. *Bull. Korean. Chem. Soc.* **2017**, *38*, 228-236.
51. Osborn, D. L.; Zou, P.; Johnsen, H.; Hayden, C. C.; Taatjes, C. A.; Knyazev, V. D.; North, S. W.; Peterka, D. S.; Ahmed, M.; Leone, S. R. The multiplexed chemical kinetic photoionization mass spectrometer: A new approach to isomer-resolved chemical kinetics. *Rev. Sci. Instrum.* **2008**, *79*, 104103.
52. Taatjes, C. A.; Meloni, G.; Selby, T. M.; Trevitt, A. J.; Osborn, D. L.; Percival, C. J.; Shallcross, D. E. Direct Observation of the Gas-Phase Criegee Intermediate (CH_2OO). *J. Am. Chem. Soc.* **2008**, *130*, 11883-11885.
53. Dodson, L. G.; Shen, L.; Savee, J. D.; Eddingsas, N. C.; Welz, O.; Taatjes, C. A.; Osborn, D. L.; Sander, S. P.; Okumura, M. VUV Photoionization Cross Sections of HO_2 , H_2O_2 , and H_2CO . *J. Phys. Chem. A* **2015**, *119*, 1279-1291.
54. Niu, D.; Shirley, D. A.; Bai, Y. High resolution photoelectron spectroscopy and femtosecond intramolecular dynamics of H_2CO^+ and D_2CO^+ . *J. Chem. Phys.* **1993**, *98*, 4377.
55. Goulay, F.; Derakhshan, A.; Maher, E.; Trevitt, A. J.; Savee, J. D.; Scheer, A. M.; Osborn, D. L.; Taatjes, C. A. Formation of dimethylketene and methacrolein by reaction of the CH radical with acetone. *Phys. Chem. Chem. Phys.* **2013**, *15*, 4049-4058.
56. Vogt, J.; Williamson, A. D.; Beauchamp, J. L. Properties and Reactions of Ketene in the Gas Phase by Ion Cyclotron Resonance Spectroscopy and Photoionization Mass Spectrometry. Proton Affinity, Site Specificity of Protonation, and Heat of Formation of Ketene. *J. Am. Chem. Soc.* **1978**, *100*, 3478.
57. Osborn, D. L., Personal communication. Sandia National Laboratories, Livermore, CA 2020.
58. Welz, O.; Zádor, J.; Savee, J. D.; Ng, M. Y.; Meloni, G.; Fernandez, R. X.; Sheps, L.; Simmons, B. A.; Lee, T. S.; Osborn, D. L., et al. Low-temperature combustion chemistry of biofuels: pathways in the initial low-temperature (550 K–750 K) oxidation chemistry of isopentanol. *Phys. Chem. Chem. Phys.* **2012**, *14*, 3112-3127.
59. Traeger, J. C.; McLoughlin, R. G.; Nicholson, A. J. C. Heat of formation for acetyl cation in the gas phase. *J. Am. Chem. Soc.* **1982**, *104*, 5318-5322.

60. Heazlewood, B. R.; Maccarone, A. T.; Andrews, D. U.; Osborn, D. L.; Harding, L. B.; Klippenstein, S. J.; Jordan, M. J. T.; Kable, S. H. Near-threshold H/D exchange in CD₃CHO photodissociation. *Nat. Chem.* **2011**, *3*, 443-448.
61. Ohno, K.; Okamura, K.; Yamakado, H.; Hoshino, S.; Takami, T.; Yamauchi, M. Penning Ionization of HCHO, CH₂CH₂, and CH₂CHCHO by Collision with He*(2³S) Metastable Atoms. *J. Phys. Chem.* **1995**, *99*, 14247-14253.
62. Egolfopoulos, F. N.; Hansen, N.; Ju, Y.; Kohse-Höinghaus, K.; Law, C. K.; Qi, F. Advances and challenges in laminar flame experiments and implications for combustion chemistry. *Prog. Energy Combust. Sci.* **2014**, *43*, 36-67.
63. Chhantyal-Pun, R.; Rotavera, B.; McGillen, M. R.; Khan, M. A. H.; Eskola, A. J.; Caravan, R. L.; Blacker, L.; Tew, D. P.; Osborn, D. L.; Percival, C. J., et al. Criegee Intermediate Reactions with Carboxylic Acids: A Potential Source of Secondary Organic Aerosol in the Atmosphere. *ACS Earth and Space Chem.* **2018**, *2*, 833-842.
64. Kroll, J. H.; Seinfeld, J. H. Chemistry of secondary organic aerosol: Formation and evolution of low-volatility organics in the atmosphere. *Atmos. Environ.* **2008**, *42*, 3593-3624.
65. Zhao, Y.; Saleh, R.; Saliba, G.; Presto, A. A.; Gordon, T. D.; Drozd, G. T.; Goldstein, A. H.; Donahue, N. M.; Robinson, A. L. Reducing secondary organic aerosol formation from gasoline vehicle exhaust. *Proc. Natl. Acad. Sci.* **2017**, *114*, 6984-6989.
66. Glowacki, D. R.; Pilling, M. J. Unimolecular Reactions of Peroxy Radicals in Atmospheric Chemistry and Combustion. *ChemPhysChem* **2010**, *11*, 3836-3843.
67. Atkinson, R. Atmospheric chemistry of VOCs and NO_x. *Atmos. Environ.* **2000**, *34*, 2063-2101.
68. Kuwata, K. T.; Hasson, A. S.; Dickinson, R. V.; Peterson, E. B.; Valin, L. C. Quantum Chemical and Master Equation Simulations of the Oxidation and Isomerization of Vinyloxy Radicals. *J. Phys. Chem. A* **2005**, *109*, 2514-2524.
69. Glowacki, D. R.; Liang, C.-H.; Morley, C.; Pilling, M. J.; Robertson, S. H. MESMER: An open-source Master Equation Solver for Multi-Energy Well reactions. *J. Phys. Chem. A* **2012**, *116*, 9545-9560.
70. Paulson, S. E.; Flagan, R. C.; Seinfeld, J. H. Atmospheric photooxidation of isoprene part II: The ozone-isoprene reaction. *Int. J. Chem. Kinet.* **1992**, *24*, 103-125.
71. Atkinson, R.; Aschmann, S. M.; Arey, J.; Shorees, B. Formation of OH Radicals in the Gas Phase Reactions of O₃ With a Series of Terpenes. *J. Geophys. Res.* **1992**, *97*, 6065-6073.
72. Grosjean, D.; Williams, E. L. I.; Grosjean, E. Atmospheric Chemistry of Isoprene and Its Carbonyl Products. *Environ. Sci. Technol.* **1993**, *27*, 830-840.
73. Neeb, P.; Moortgat, G. Formation of OH Radicals in the Gas-Phase Reaction of Propene, Isobutene, and Isoprene with O₃: Yields and Mechanistic Implications. *J. Phys. Chem. A* **1999**, *103*, 9003-9012.
74. Malkin, T. L.; Goddard, A.; Heard, D. E.; Seakins, P. W. Measurements of OH and HO₂ yields from the gas phase ozonolysis of isoprene. *Atmos. Chem. Phys.* **2010**, *10*, 1441-1459.
75. Gutbrod, R.; Kraka, E.; Schindler, R. N.; Cremer, D. Kinetic and theoretical investigation of the gas-phase ozonolysis of isoprene: Carbonyl oxides as an important source for OH radicals in the atmosphere. *J. Am. Chem. Soc.* **1997**, *119*, 7330-7342.
76. Gutbrod, R.; Meyer, S.; Rahman, M. M.; Schindler, R. N. On the use of CO as Scavenger for OH radicals in the Ozonolysis of Simple Alkenes and Isoprene. *Int. J. Chem. Kinet.* **1997**, *29*, 717-723.
77. Paulson, S. E.; Chung, M.; Sen, A. D.; Orzechowska, G. Measurement of OH radical formation from the reaction of ozone with several biogenic alkenes. *J. Geophys. Res.* **1998**, *103*, 25533-25539.
78. Rickard, A. R.; Johnson, D.; McGill, C. D.; Marston, G. OH Yields in the Gas-Phase Reactions of Ozone with Alkenes. *J. Phys. Chem A* **1999**, *103*, 7656-7664.
79. Donahue, N. M.; Kroll, J. H.; Anderson, J. G.; Demerjian, K. L. Direct observation of OH production from the ozonolysis of olefins. *Geophys. Res. Lett.* **1998**, *25*, 59-62.

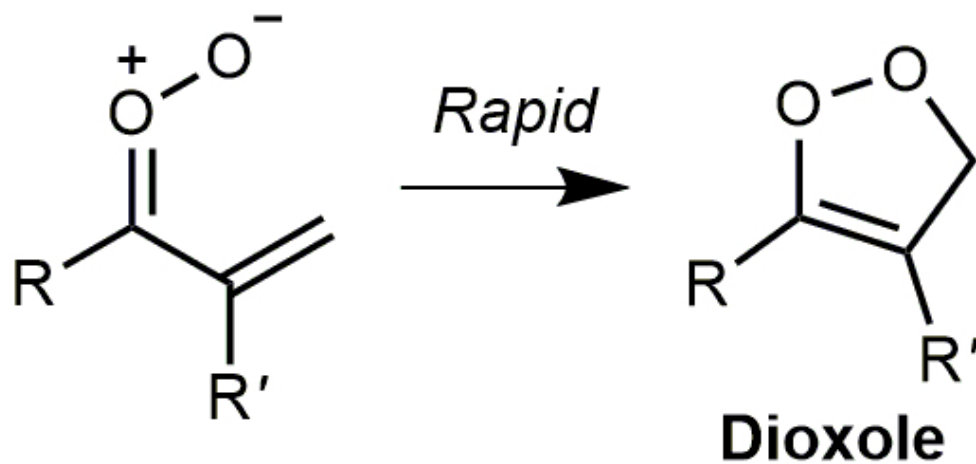
- 1
2
3 80. Atkinson, R.; Baulch, D. L.; Cox, R. A.; Crowley, J. N.; Hampson, R. F.; Hynes, R. G.; Rossi, M.
4 J.; Troe, J.; Subcommittee, I. Evaluated kinetic and photochemical data for atmospheric chemistry:
5 Volume 2 – gas phase reactions of organic species. *Atmos. Chem. Phys.* **2006**, *6*, 3625-4055.
6 81. Master chemical mechanism, MCM v3.2. <http://mcm.leeds.ac.uk/MCM>. (accessed March 10,
7 2020).
8 82. Baulch, D. L.; Cobos, C. J.; Cox, R. A.; Esser, C.; Frank, P.; Just, T.; Kerr, J. A.; Pilling, M. J.;
9 Troe, J.; Walker, R. W., et al. Evaluated Kinetic Data for Combustion Modelling. *J. Phys. Chem. Ref.*
10 *Data* **1992**, *21*, 411-734.
11 83. Maity, S.; Kaiser, R. I.; Jones, B. M. Formation of Ketene (H_2CCO) in Interstellar Analogous
12 Methane (CH_4)-Carbon Monoxide (CO) Ices: A Combined FTIR and Reflectron Time-of-Flight Mass
13 Spectroscopic Study. *Astrophys. J.* **2014**, *789*, 1-13.
14
15
16
17
18
19
20
21
22
23
24
25
26
27
28
29
30
31
32
33
34
35
36
37
38
39
40
41
42
43
44
45
46
47
48
49
50
51
52
53
54
55
56
57
58
59
60





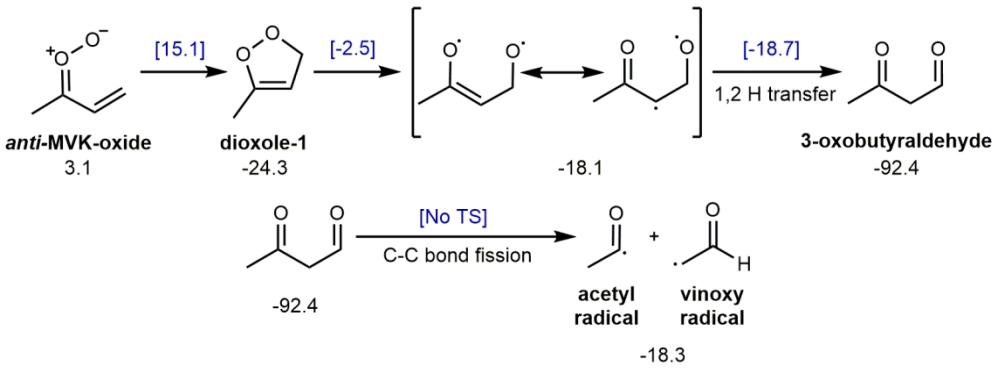
Scheme 1

109x44mm (300 x 300 DPI)



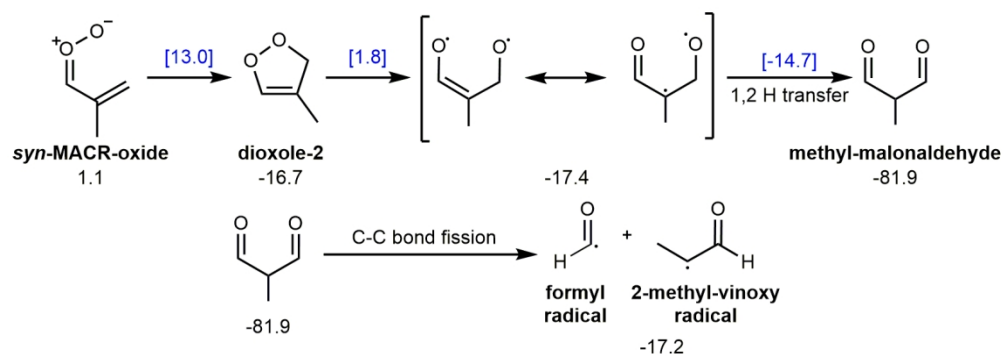
Scheme 2

44x22mm (300 x 300 DPI)



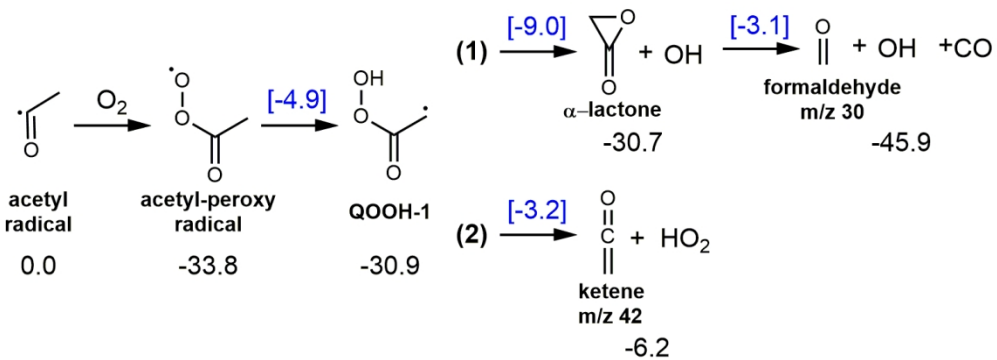
Scheme 3

139x51mm (300 x 300 DPI)



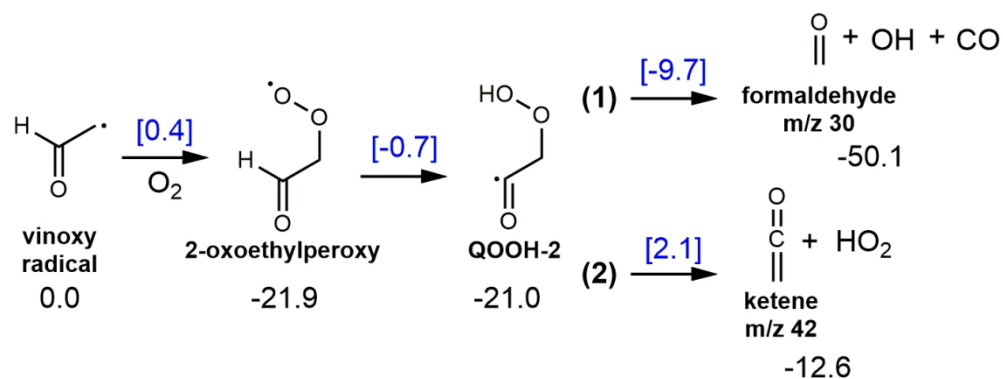
Scheme 4

144x51mm (300 x 300 DPI)



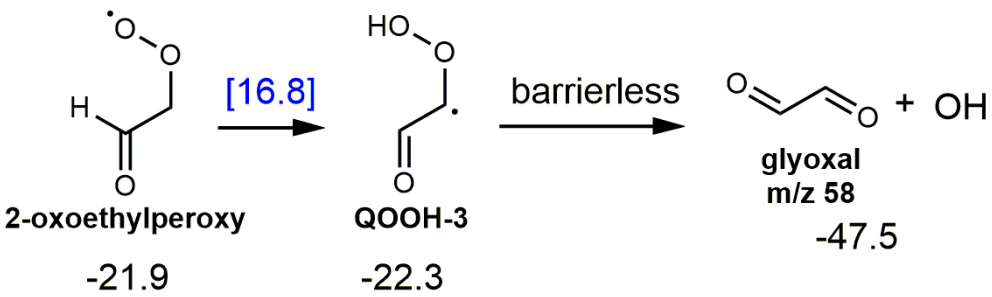
Scheme 5

134x49mm (300 x 300 DPI)



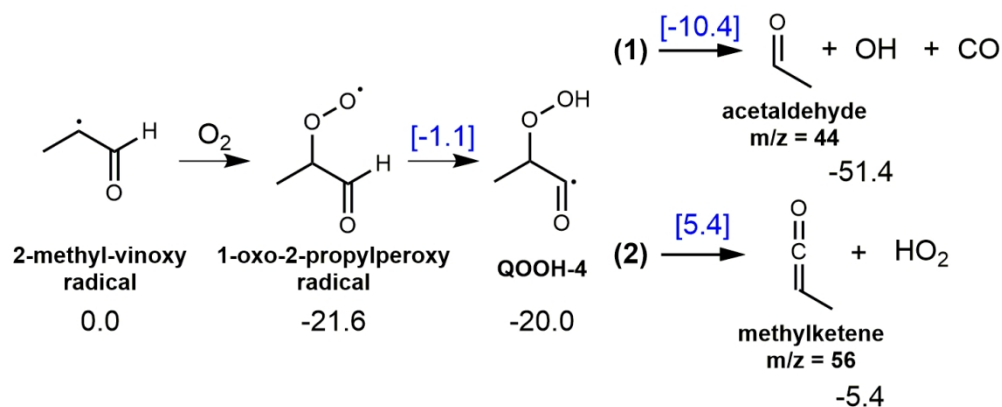
Scheme 6

119x46mm (300 x 300 DPI)



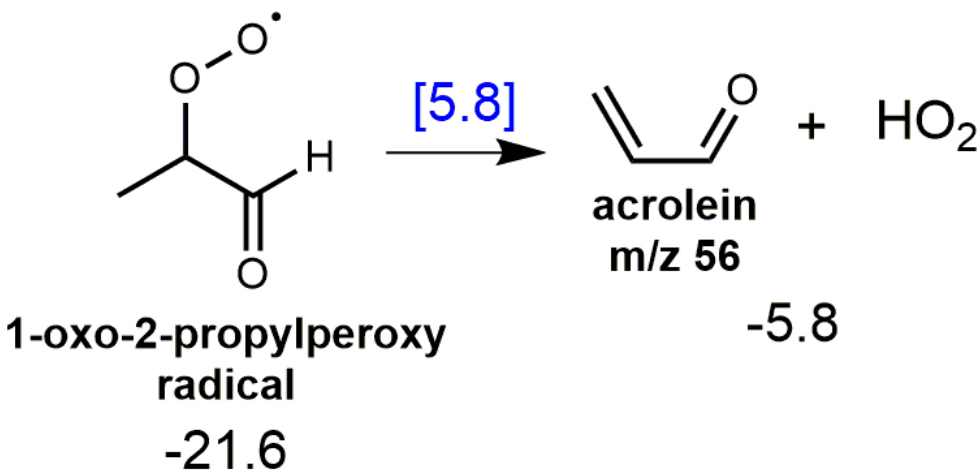
Scheme 7

96x29mm (300 x 300 DPI)



Scheme 8

123x51mm (300 x 300 DPI)



Scheme 9

64x32mm (300 x 300 DPI)

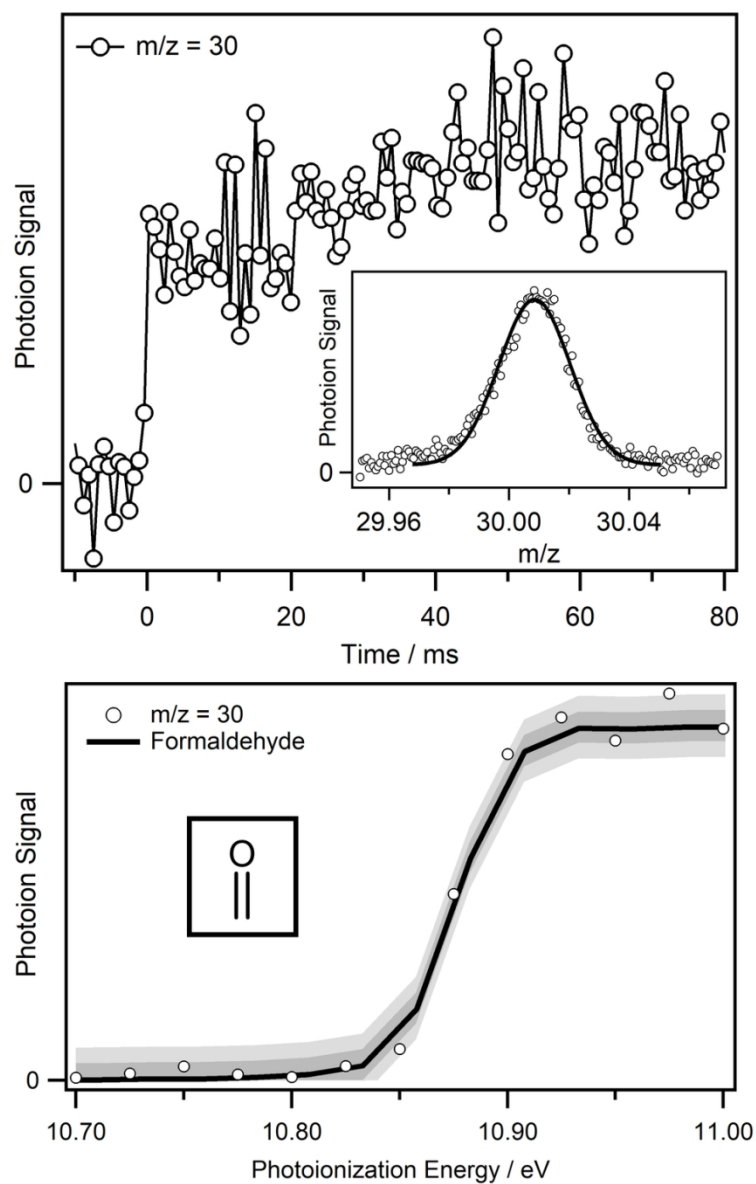


Figure 1

85x134mm (300 x 300 DPI)

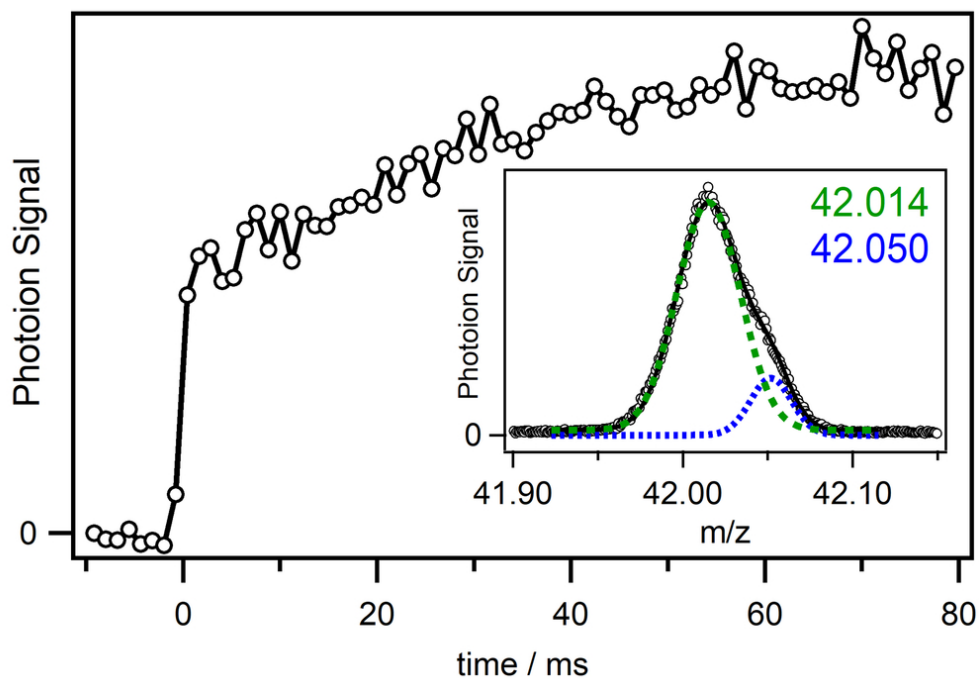


Figure 2

85x60mm (300 x 300 DPI)

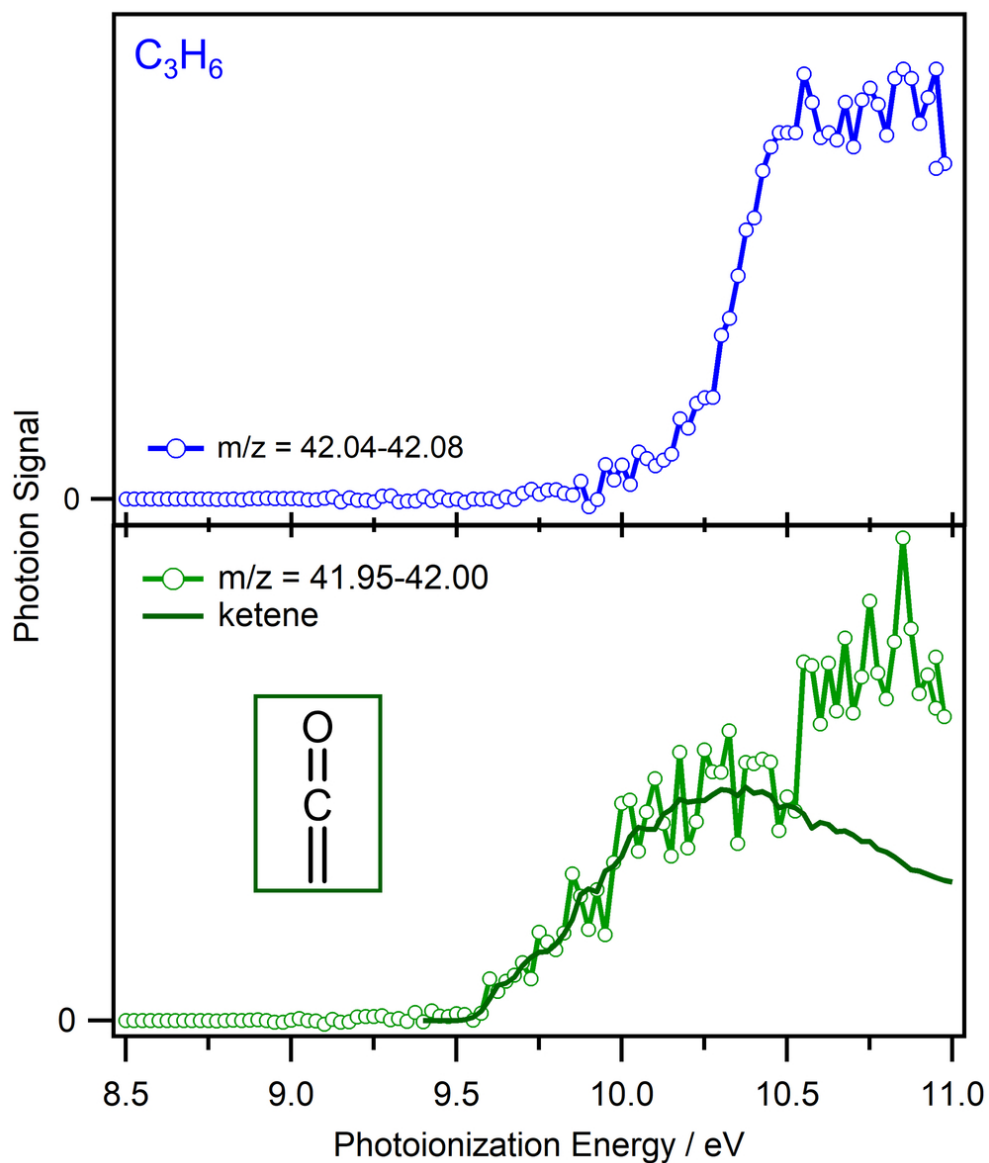


Figure 3

85x101mm (300 x 300 DPI)

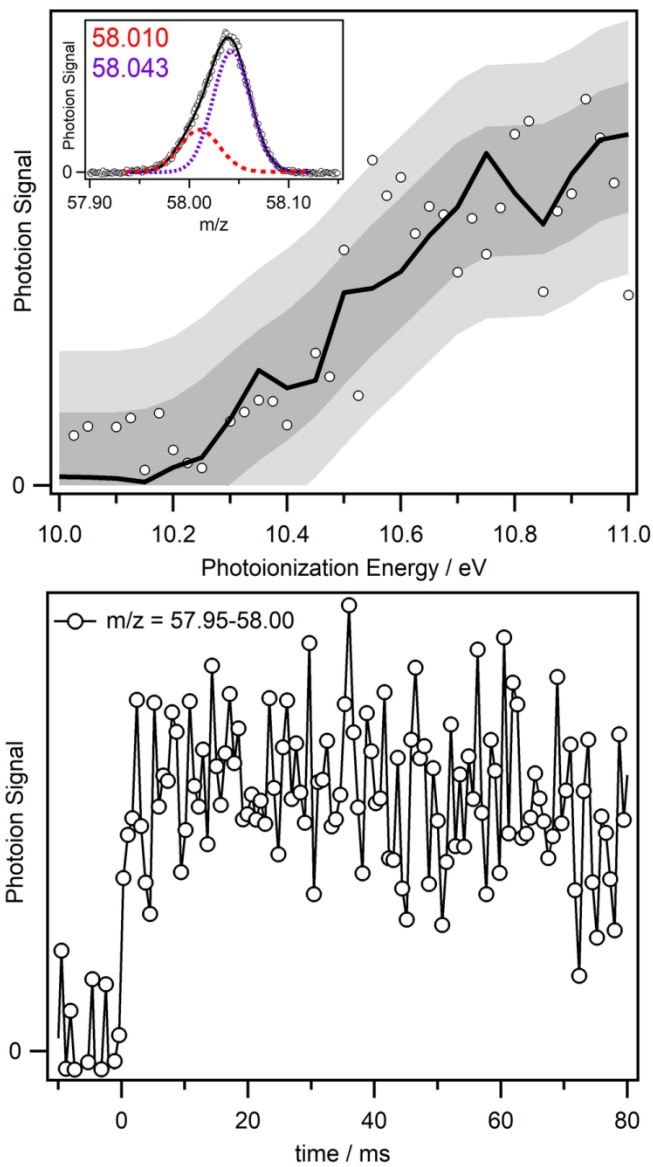


Figure 4

85x155mm (300 x 300 DPI)

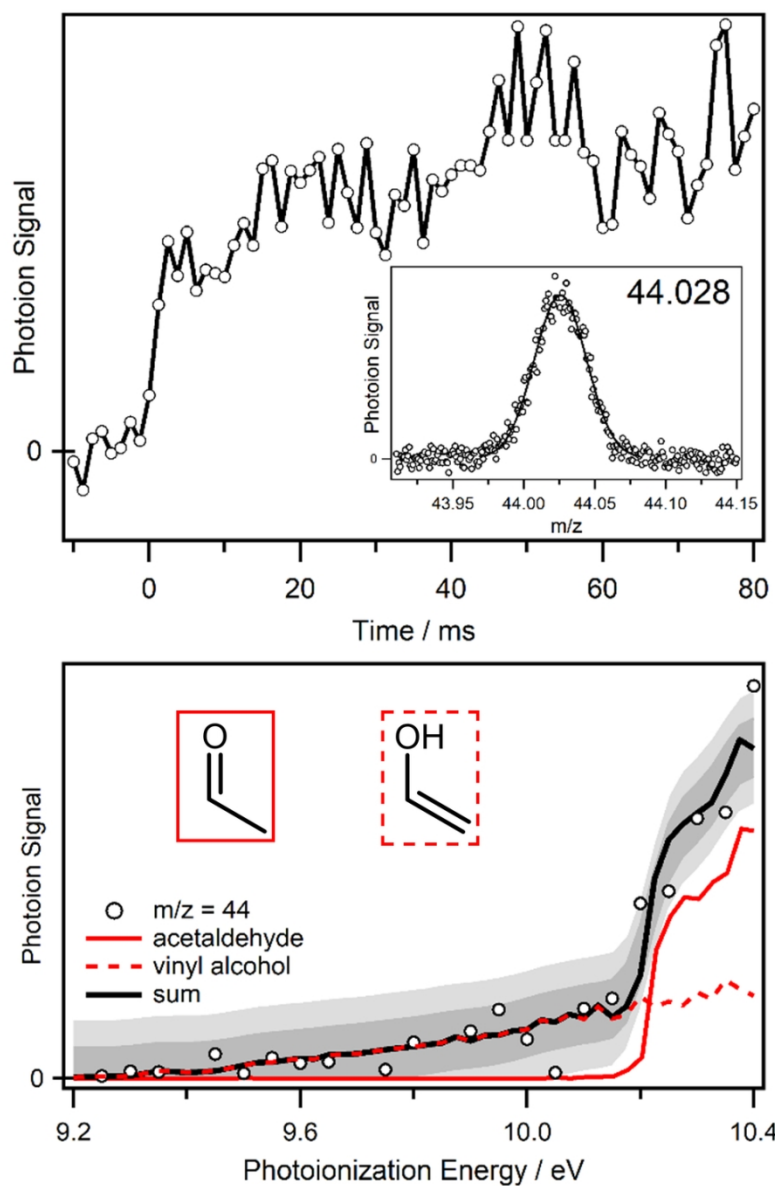


Figure 5

85x128mm (300 x 300 DPI)

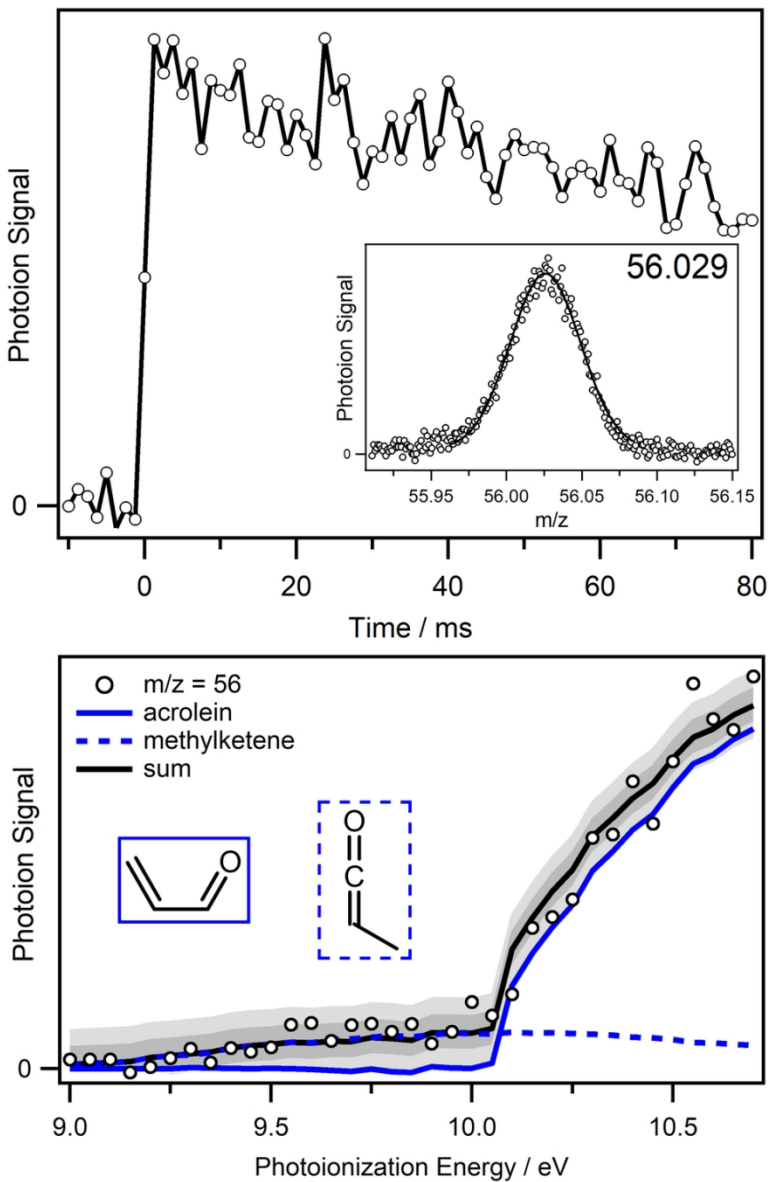


Figure 6

85x129mm (300 x 300 DPI)

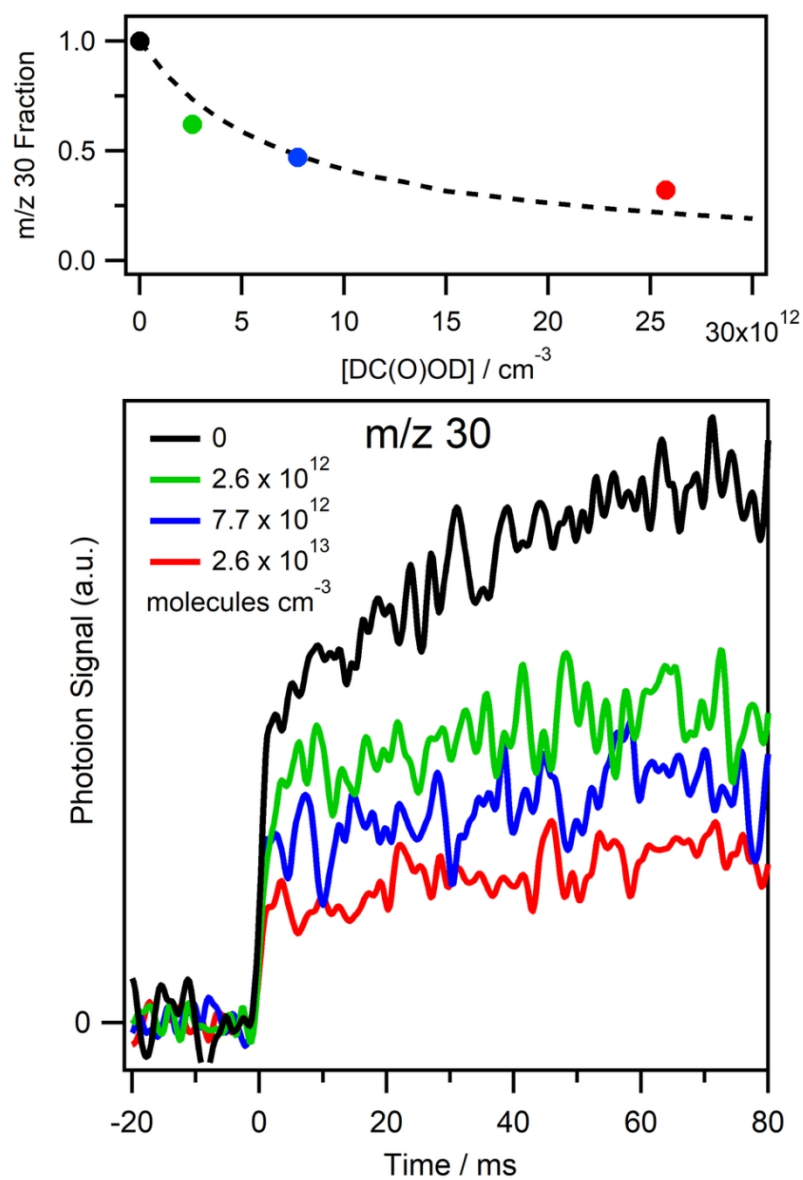
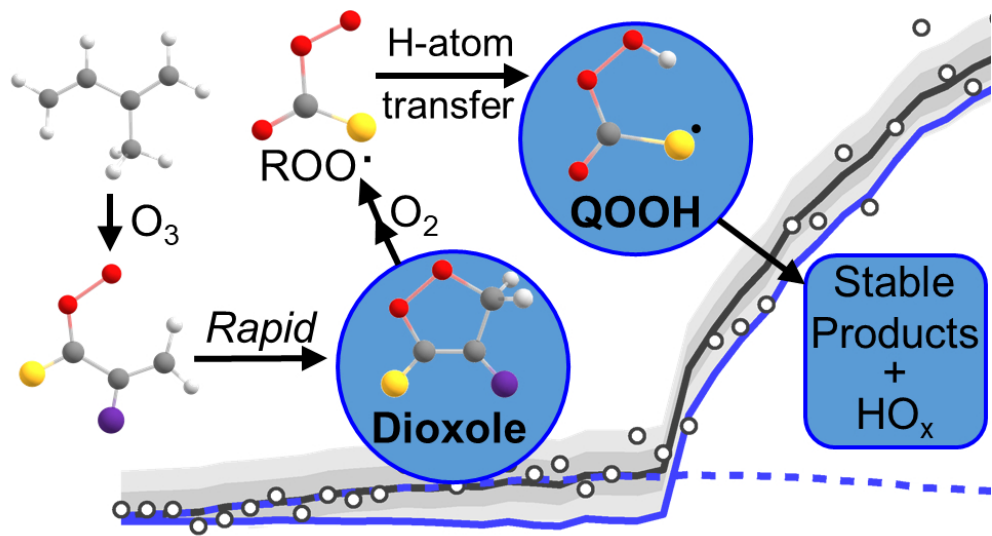


Figure 7

85x121mm (300 x 300 DPI)



TOC graphic

82x44mm (300 x 300 DPI)